Birzeit University

Department of Physics

Electron Dynamics in a Single C_{60} Molecule

Co-Supervisors:
Prof. Dr. Wael Karain
Prof. Dr. Matthias Kling

Author:
Mohammed Qahosh

Committee members:
Dr. Hazem Abusara
Dr. Khaled Eid

This Thesis was submitted in partial fulfillment of the requirements for the Master of Science Degree in physics From the Faculty of Graduate Studies at Birzeit University

January 2020

Electron Dynamics in a Single C_{60} Molecule

By

Mohammed Qahosh

Accepted by the Faculty of Graduate Studies, Birzeit University, in partial fulfilment of the requirements of the Master's Degree in Physics.

Thesis committee:

Prof. Dr. Wael Karain and Prof. Dr. Matthias Kling (Co-Supervisors)

Dr. Hazem Abusara (Member)

Dr. Khaled Eid (Member)

January 2020

Acknowledgements

This work would not have been possible without the financial support of the Vice President for Academic Affairs, Prof. Dr. Henry Giacaman, and the Ludwig Maximilian University of Munich for the research scholarship.
I would like to express my deep gratitude to Prof. Dr. Wael Karain and Dr. Hirofumi Yanagisawa, my research supervisors, for their patient guidance, enthusiastic encouragement and useful critiques of this research work.
Besides my advisors, I would like to thank the rest of my thesis committee: Dr. Hazem Abusara and Dr. Khaled Eid, for their encouragement, insightful comments.
Special thanks for Prof. Dr. Matthias King, our group leader, for his support where he used to be my reference in times of stress.

Nobody has been more important to me in the pursuit of this project than the members of my family. Words can not express how grateful I am to my mother and father for all of the sacrifices that you have made on my behalf. Your prayer for me was what sustained me thus far. I would also like to thank my beloved fiance, my sisters and my brothers for encouraging me throughout this experience.

Abstract

Applying a strong DC field at a metal surface deforms the surface potential barrier, enabling electrons to tunnel through the deformed barrier into vacuum. This phenomenon is called field emission (FE). If a high negative bias is applied to a nano-metric sharp tip, electrons can be emitted due to FE. The emitted electrons radially propagate and are collected on a counter electrode (phosphor screen). A magnified emission map from the tip apex will be displayed on the phosphor screen, enabling us to distinguish single molecule deposited onto the tip surface. This technique is called field emission microscope (FEM).

No matter what kind of molecules deposited over the nano-tip, cloverleaf patterns appear on the phosphor screen. Each cloverleaf pattern is considered to represent single molecule. The origin of these clover leaves, however, still unknown. At room temperature, these patterns are unstable since C_{60} molecules are very mobile on the nano-tip. This makes it hard to clarify the mechanism forming these clover leaves. In this thesis we would like to stabilize these patterns to provide a better condition for further studies. In order to do that, we will cool the tip down to 90 Kelvin via a newly designed cooling system using liquid nitrogen. Fowler and Nordheim (F-N) plot was recorded to characterize the nano-tip surface.

Different amounts of C_{60} were deposited onto tungsten or tungsten carbide nano-tip, and the dynamics of C_{60} over these two kinds of surfaces were studied. When the tip is highly covered with C_{60} we could observe the cloverleaf patterns in a reproducible manner. We could also see the two-cloverleaf pattern onto the tungsten carbide surface even in the low coverage, which has not been observed before. However, we could not see this pattern on the tungsten surface. At low temperature, we observed that C_{60} molecules on the nano-tip became very stable. We could also observe transformation of a four-cloverleaf pattern into a circular pattern while cooling the nano-tip.

We determined slopes of F-N plots taken from a clean nano-tip and compared them with the slopes for the electron emission from single C_{60} on the nano-tip. At room temperatures, previous studies showed that slope of F-N plot behaves randomly. In our study, we could also find the random behavior of the F-N plot slopes at room temperature. Similar plots were taken at low temperature in the low and high coverage regimes. The results showed a random behavior of the F-N plot slopes, which is the same behavior at the room temperature. From this random behavior of the slopes of F-N plots, we concluded that F-N plot is not affected by the mechanical stability of C_{60} molecules.

مُلَخَّص

التأثيرُ بمجالٍ كهربائيٍ قوي على سطحِ معدنٍ يعيدُ تشكيلَ حاجزِ الطاقةِ للسطحِ ممكِّنا الإلكترونات من اختراقهِ كمياً إلى الفراغ. هذه الظاهرة تُسمّى بمجالِ الإلكترونات المنبعثة (FE). إذا تم استخدام قطبية سالبة على رأس سلك مدبب إلى المستوى النانومتري، فهذا يُمكِّنُ الإلكترونات من الانبعاث من هذا الرأس نتيجةً لظاهرة (FE). تسير هذه الإلكترونات المنبعثة في الفراغ بشكلٍ قطري حيث يتم تجميعها على قطبٍ موجبٍ (شاشة فسفور) مشكلةً صورةً مكبَّرة لقمةِ الرأسِ المدببِ، وهذا بدوره يساعدنا في تمييز جزيء واحدٍ موضوعٍ على سطح الرأسِ المدببِ. يُطلَقُ على هذه التقنيةِ بمجهرِ رصدِ الإلكتروناتِ المنبعثةِ (FEM).

بغض النظرِ عن نوعِ الجزيئاتِ التي يتم وضعها على سطحِ الرأسِ المدببِ، يتمُّ مشاهدة أنماطٍ تُسمّى (Clover leaves) على الشاشة الفسفورية. كل نمطٍ من هذه الأنماطِ يُعتَقَدُ بأنّه يُمثِّلُ جزيئاً واحداً. على الرغم من هذا، فإن سرَّ تشكُّلِ هذه الأنماطِ غيرُ معروفٍ إلى وقتنا هذا. **على درجاتِ حرارةِ الغرفةِ فإن هذه الأنماطَ غيرُ مستقرةٍ**، لأن جزيئاتِ (C_{60}) ذو ديناميكيةٍ حركيةٍ عاليةٍ. هذا بدوره يُصَعِّبُ مهمةَ اكتشافِ سرِ تشكُّلِ هذه التراكيب. في بحثنا هذا **سنقوم بمحاولةِ جعلِ هذه التراكيبِ أكثرَ استقراراً** لتوفير ظروفٍ أفضلَ لإجراءِ دراساتٍ مستقبليةٍ أملاً في إكتشاف سرِّ تشكُّلِ هذه الأنماط. لكي نتمكن من ذلك، **سنقوم بتبريد الرأسِ المدبَّبِ إلى درجة حرارة ٩٠ كلفن** باستخدام نظام تبريد جديد تم تصميمه خصيصاً لهذه التجربةِ مستخدمين سائلَ النيتروجين. لقد قمنا أيضاً بدراسةِ سطحِ الرأسِ المدببِ باستخدام طريقة (F-N) Fowler and Nordheim.

كميات مختلفة من جزيئات C_{60} تم تبخيرها و إيداعها على قمةِ طرفِ سلكِ التنجستن W أو كربيد التنجستن (WC, W_2C) النانومتريّ، وقمنا بدراسة سلوك هذه الجزيئات على هذين السطحين. عندما يكون الرأسُ النانومتريُّ مغطىً بكمياتٍ كبيرةٍ من جزيئات C_{60} تمكنا من مشاهدة تشكل أنماط (Clover leaves) بشكلٍ متكررٍ. كما **تمكنا ولأولِ مرةٍ من ملاحظةِ تشكلِ نوعٍ من هذه الأنماطِ يُسمَّى (Two-cloverleaf) على سطحِ كربيدِ التنجستن النانومتريّ عندما يكون السطحُ مغطًىً بكمياتٍ قليلةٍ من جزيئات C_{60} وهذا ما لم يتم ملاحظتهَ في الدراساتِ السابقة**. إلا أنّنا لم نتمكن من مشاهدةِ هذا النمط على سطح التنجستن النانومتريّ. **على درجاتِ حرارةٍ منخفضةٍ لاحظنا أن جزيئات C_{60} تصبح مستقرةً على السطح النانومتري**. كما وتمكنا من ملاحظةِ تحولِ نمط (Four-cloverleaf) إلى نمطٍ دائريٍ خلال عمليةِ تبريدِ الرأسِ النانومتريِّ.

لقد قمنا بإيجاد مَيلِ رسومات (F-N) تم أخذها من سطحِ الرأسِ النانومتريِّ النظيف ومقارنتها بمَيلِ رسوماتٍ لانبعاث الإلكترونات من جزيء C_{60} على هذه السطوح. على درجةِ حرارةِ الغرفةِ، بَيَّنَت الدراساتُ السابقةُ أنّ تصرفَ مَيلِ هذه الرسوماتِ يكون عشوائياً، وهذا ما لاحظناه أيضا في دراستنا لهذا السلوكِ على درجةِ حرارةِ الغرفة. رسوماتٌ مشابهةٌ تم أخذها من السطحِ المغطى بكميات مختلفة من جزيئات الكربون على درجةِ حرارةٍ منخفضةٍ بعد تبريد الرأس وشاهدنا أيضا تصرفاً عشوائياً للمَيلِ مشابهاً للتصرفِ على درجةِ حرارةِ الغرفة. من هذا السلوكِ العشوائي لميلِ رسومات F-N على درجة حرارة الغرفة و على درجاتِ حرارةٍ منخفضةٍ فإننا نستنتج بأنّ طريقةَ (F-N) لا تتأثرُ بالاستقرارِ الديناميكيِّ لجزيئات C_{60}.

Contents

List of Figures

Chapter 1

Introduction

Emission of electrons from cold metals was first described by R.W. Wood [1] in 1897, where this phenomena was happening in early experiments when high voltages were applied to highly sharpened cathodes. In 1922, Lilienfeld [2] detected an unpredictable current on the order of milliamperes once a strong electric field was applied in the evacuated tube. Schottky [3], in 1923, suggested a possible connection with thermionic emission, to be the first person who tried to explain cold field emission, by proposing that an external electric field reduces the height of the potential barrier at the metal surface and the work function respectively. Based on his proposal, there is a significant dependence upon temperature by the emitted current, and a linear relationship between log of the current density and the square root of the applied voltage is expected. However, Gossling [4], and Millikan and Eyring [5] showed that field current, and temperature, independence. Millikan and Lauritsen [6] found a straight line relation between log (field intensity) and the inverse of the field. They tried to explain field emission and thermionic emission in one formula. This formula worked for high fields and low temperatures, and high temperatures and low fields, but not in the in between case. In 1928, Sommerfeld's electron theory of metals was used to explain the field emission using the quantum theory. Fowler and Nordheim [7] used the Fermi-Dirac statistics for the energy distribution of metal electrons to calculate the number of electrons in each energy range arriving the potential barrier. They multiplied this by the penetration probability, and derived a formula for the current density. Nordheim [8] revised the calculation to include the effect of Schottky's image force.

A revolution in the field emission started in 1937 when Muller [9, 10] invented the field emission microscope. His device consisted of a negatively biased tip , and a fluorescent screen at anode potential in front of the tip. When electrons are emitted from the tip, due to the strong field, they travel almost radially, as the tip is an equipotential metal surface, and hence a magnified image of the cathode surface geometry could be shown on the screen. He also initiated a new research field when he started depositing molecules onto the nano-tip; where in 1950 he could record the first ever image of deposited Copper Pthalocyanines molecules onto a 200nm radius of carvature tungsten tip using the field emission microscope technique [11]. Afterwards, different kinds of molecules have been deposited and field emission was investigated. One fascinating phenomenon is the appearance of a well distinct and interesting pattern, called clover leaves, no matter what molecules are deposited [12,

13, 14, 15].

As the field emission patterns are not stable at room temperature, it is not easy to discover the origin of reproducible patterns with specific symmetries called cloverleaves where each cloverleaf is considered to represent a single molecule. In this work we would like to stabilize FE patterns to provide a better condition for further studies. In order to do that we will cool the tip to decrease the mobility of C_{60} molecules on the nano-tip. We will also use Fowler-Nordheim plot to analyse the nano-tip surface.

In the first chapter, I will discuss the main physical concepts necessary for this research. In the second chapter I will show our main setup used for this work, focusing on the self designed cooling system used to cool the tip down to 90 Kelvin using liquid nitrogen. Afterwards, in the third chapter I will explain the starting point for our experiments which is cleaning the nano-tip to end up with a well recognized clean tungsten surface. After that, C_{60} was deposited in different amounts by using a timer and controlling the evaporation temperatures. In the forth chapter, we moved into another surface called tungsten carbide, where depositing large amounts of C_{60} onto the tungsten surface and then flash heating the tip gradually transfer the tungsten surface into tungsten carbide surface. Similar kind of experiments were done on these two kinds of surfaces. In the fifth chapter I will talk about the main idea of this research which is studying the effect of low temperatures on the behaviour of C_{60} covering the nano-tip. The tip was highly covered with C_{60} and then cooled using liquid nitrogen. The surface was also analyzed using the F-N plot method at room temperature and after cooling. Finally an outlook is proposed which has an idea that could be used to clarify the origin of the cloverleaf patterns.

Chapter 2

Physical Concepts

2.1 Field Emission From Metals

Field emission is tunneling of electrons through a deformed potential barrier at the metal surface into vacuum under the influence of a high electric field [16] as indicated by Fig. 2.1a. This differs from thermionic emission and photoemission, where electrons are given enough energy to overcome the potential barrier at the metal surface.

In the absence of an external electric field, the thermal energy of the electrons is not enough to pass over the barrier and will be trapped within the metal, as Fig. 2.1a shows. When the field is applied, the potential barrier at the metal surface is deformed. It corresponds to an electron potential in the vacuum containing an electric field of strength **F**, and this comes up with an abrupt potential step at the metal surface forming a triangular barrier, as can be seen by Fig. 2.1b Based on quantum theory, unexcited electrons can leak out(tunnel) through it.

Now, once an electron has tunneled into vacuum and is at a distance x from the metal surface, an attraction results between the tunneled electron and the positive charge induced on the metal surface. This would be equivalent to an attraction force between the emitted electron in the vacuum and a positron existing at a distance -x within the metal surface. The attraction force is given by the classical Coulomb's law:

$$F_{attraction} = \frac{e^2}{2x.2x} \tag{2.1}$$

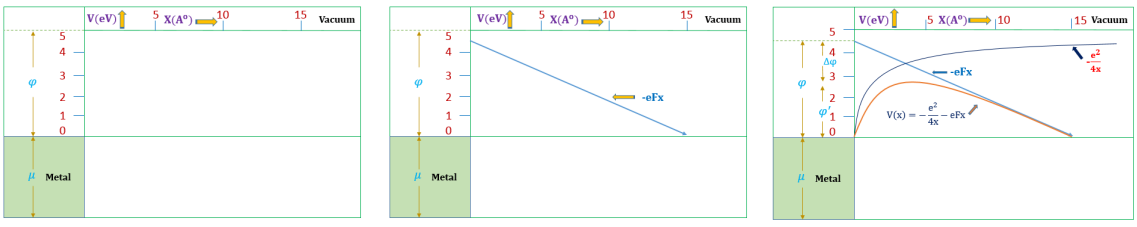

Figure 2.1: Potential energy diagram for electrons at a metal surface: ϕ, work function; μ, Fermi energy; ϕ', real work function; $\Delta\phi$, decrease in work function due to image potential; $x = 0$, metal surface (a) without the electric field; (b) in the presence of electric field without image potential; (c) with an electric field and image potential

and the potential energy is:

$$V = \frac{-e^2}{4x} \tag{2.2}$$

Hence, electron feels two potential energies: the external and the image potential, i.e. the resultant potential barrier is:

$$V = -\mathbf{F}ex + \frac{-e^2}{4x} \tag{2.3}$$

So, the potential barrier near the surface is decreased even more by the image potential, and there is no vertical rise anymore at the metal surface, as one can see from Fig. 2.1c.

This means that a stronger applied external electric field, and a thinner and lower potential barrier at the metal surface, lead to a larger emitted electron current.

2.2 Condition for Field Emission

As the number of quantum states near the Fermi level is much more than that near the bottom of the conduction band, we expect mainly the energy levels near the top of the Fermi sea μ or ϵ_{fermi} to be involved in electron emission [17]. Based on this fact, it is enough to concentrate on electrons near the Fermi level. The uncertainty in momentum of such an electron corresponds to a barrier of height ϕ, is

$$\Delta p = \sqrt{2m\phi} \tag{2.4}$$

Using the Heisenberg uncertainty principle, the corresponding uncertainty in the position of that electron, is,

$$\Delta x = \frac{\hbar}{2\sqrt{2m\phi}} \tag{2.5}$$

If this is of the order of magnitude of the barrier width,

$$x = \frac{\phi}{\mathbf{F}e} \tag{2.6}$$

the probability for the electron to tunnel into vacuum is significant. This would be achieved if the following equation is satisfied,

$$\frac{\phi}{\mathbf{F}e} = \frac{\hbar}{2\sqrt{2m\phi}} \tag{2.7}$$

or

$$\mathbf{F} = 2\sqrt{\frac{2m}{\hbar^2}}\frac{\phi^{\frac{3}{2}}}{e} \tag{2.8}$$

For tungsten using ϕ =4.5 eV, the required field for electrons to tunnel into vacuum is $10^7 \frac{V}{cm}$. Then, electrons need to tunnel through a potential barrier of width 15 Angstrom.

2.3 The Field Emission Microscope

The field emission microscope is the leading application of cold field emission. It is used to study the structures of molecular surfaces. Emission of electrons from an emitter is used by this technique to produce a magnified image on a fluorescent screen for the surface of the emitter.

Fields of the order of $10^7 \frac{V}{cm}$ are needed to achieve the required field emission [16] as I showed in the previous section. To achieve such high fields, regions of high curvature are needed to increase the field at the surface, where a wire is etched typically to a very sharp tip. After evacuating the system to pressures of order of 10^{-10} mbar, the tip is heat polished electrically in vacuum. This emits contaminants from the surface of the tip, producing a smooth hemispherical shape with lower surface energy to facilitate the emission of electrons from the tip.

Now, if the hemispherical emitter is surrounded by a spherical anode in the form of a fluorescent screen, then a Field Emission Microscope is formed. Fig. 2.2 is a schematic drawing of the FEM.

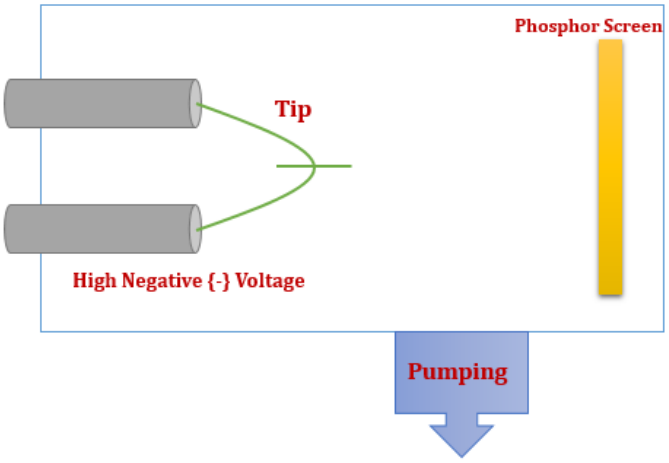

Figure 2.2: Schematic diagram of the Field Emission Microscope

If the tip apex were a sphere with radius r and voltage V, then the field at its surface would be,

$$\mathbf{F} = \frac{V}{r} \tag{2.9}$$

However, the tip has the shape of a hemisphere mounted on a cylindrical support. Thus, the field at the tip apex surface is reduced by a factor k$\approx$ 5* [17] near the symmetry axis of the tip apex and increases with polar angle. Hence, this comes up with a field,

$$\mathbf{F} = \frac{V}{k * r} \tag{2.10}$$

at the tip surface.

(k value depends on the exact geometry of the tip).

Based on equation 2.10 using 1 kV tip voltage with 1000A^o radius of curvature is enough to achieve the required field emission.

2.4 Basics of Image Formation

The Tungsten, being a metal, is a conductor and hence an equipotential surface. The lines of force at the surface are orthogonal to it. The kinetic energy of the electrons that have just penetrated the potential barrier at the tungsten surface is very small. Therefore, the emerged electrons will follow the lines of force starting from the tungsten surface, as can be seen from Fig. 2.3 When these electrons reach the fluorescent screen, and since each emitted electron produces a glowing spot, a very large magnified image will be formed.

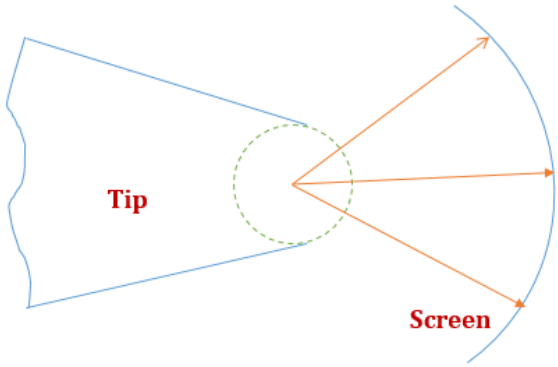

Figure 2.3: Schematic diagram showing the track of an emerged electron form the tip.

Heating the tip to high temperatures to clean it, smooths its surface to the atomic level. The resultant emitter apex is now composed of various flats corresponding to different crystallographic orientations and Miller indices.

If the work functions of every tiny spot on the tip apex were the same, the pattern on the screen would simply be a circular big spot without variations in the intensity. However, since different faces correspond to different work functions, and the emission current is a Fowler and Nordheim-work function exponential dependent, details are in sec. 2.6, any slight local variation in the work function results in noticeable differences in the intensity of the emission current. This is seen clearly on the fluorescent screen pattern.

Based on the previous discussion, the pattern appears on the screen is a magnified emission map of the tip apex and a reflection of the variations in the work functions of different faces of the tip apex [18, 19].

If r is the tip radius and x is the distance from the tip to the screen ($\sim$ 4cm) then, the magnification would be $\frac{x}{r}$. But, since we do not have a perfect spherical emitter, the emitter shank compresses the lines of force resulting in an actual magnification of $\frac{x}{Br}$,where B $\sim$ 1.5 is the compression factor [20].

2.5 Local Magnification

Local work function variations result in emission current intensity differences. In addition, changes in the emission may also be due to electric field local enhancement wherever asperities or protuberances exist on the original tip [17].

In the vicinity of these asperities equipotentials will be compressed. For the force lines to stay orthogonal to these compressed surfaces, these lines must diverge more at these "independent bumps". The more the divergence of the lines and the emitted electrons respectively, the larger the magnified spot caused.

Hence, this picture is equivalent to a very small independent tip superimposed over the main tip, as shown in Fig. 2.4. This causes local field enhancement and more magnification compared with that from the principal tip.

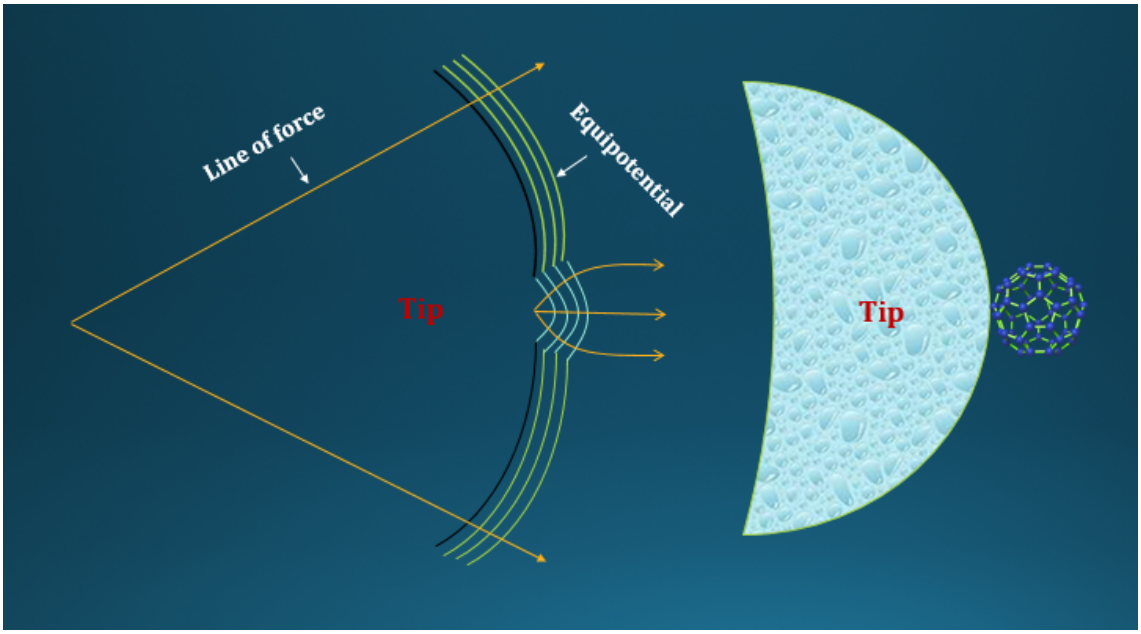

Figure 2.4: Schematic diagram showing the local enhancement in the vicinity of the small tip superimposed over the original tip

Rose [21] did the calculation for the magnification in such case:

$$M^{'} = 1.1(\sqrt{\frac{r}{R}})M_o \tag{2.11}$$

Where M_o is the normal magnification from the main tip and r is its radius. While, $M^{'}$ is the magnification from the superimposed tip and R is its Radius.

If we consider a C60 molecule as a small bump with diameter $\sim 10A^o$ superimposed over a main tip of radius 1000 A^o we would be able to get a relative magnification of $\sim$ 15 times.

2.6 The Fowler-Nordheim Equation

Tunneling of electrons from a metal surface into vacuum was formulated by Fowler and Nordheim resulting with the F-N equation. If electrons were tunneling from an exact triangular potential barrier as in Fig. 2.1b excluding the image effect, the F-N equation would be

$$J = 6.2 \times 10^6 \frac{(\mu/\phi)^{1/2}}{(\mu+\phi)} F^2 exp[-6.8 \times 10^7 \frac{\phi^{3/2}}{F}] \frac{amp}{cm^2} \tag{2.12}$$

for energies in electron volts and electric field F in volts per centimeter; (we need to remember that F is the local electric field at the nano-tip surface). Here, μ is the Fermi energy, ϕ is the work function of the metal and J is the field emission current density in amp/cm^2.

Now, taking into consideration the image effect as shown in Fig. 2.1c the F-N equation takes the form

$$J = 6.2 \times 10^6 \frac{(\mu/\phi)^{1/2}}{\alpha^2(\mu+\phi)} F^2 exp[-6.8 \times 10^7 \frac{\phi^{3/2}\alpha}{F}] \frac{amp}{cm^2} \tag{2.13}$$

where α is the image correction term

$$\alpha = (1-y)^{1/2} = (1 - 3.8 \times 10^{-4}(F^{1/2}/\phi))^{1/2} \tag{2.14}$$

Detailed derivation of the F-N equation can be found in literature [20]. Equation 2.13 can be written as

$$J = a\phi^{-1} P_f F^2 exp[-b\frac{\phi^{3/2}}{F}] \tag{2.15}$$

where P$_f$ is the prefactor given by

$$P_f = 4\phi^{3/2}\mu^{1/2}/(\phi+\mu) \tag{2.16}$$

P$_f$ can be set to unity as it is of the order of unity [22]. Then,

$$J = a\phi^{-1} F^2 exp[-b\frac{\phi^{3/2}}{F}] \tag{2.17}$$

where a and b are constants (a=1.54$\times$10^{-6}AeVV^{-2}, b=6.83V$^{-3/2}$Vnm^{-1}) [22].

If our nano-tip (cathode) is at a distance d away from the anode, and a potential difference V is applied between them, then the macroscopic electric field **F** is,

$$\mathbf{F} = \frac{V}{d} \tag{2.18}$$

However, due to the enhancement at the surface of the nano-tip, the local electric field F can be much higher that the macroscopic electric field **F**, such that

$$F = \beta \mathbf{F} \tag{2.19}$$

where β is the field enhancement factor. Thus, by combining equations 2.18 and 2.19, the image potential corrected F-N equation can be written in terms of the macroscopic electric field $\mathbf{F}$,

$$J = a\phi^{-1}\mathbf{F}^2 exp[-\frac{b\phi^{\frac{3}{2}}}{\beta\mathbf{F}}] \tag{2.20}$$

A standard method to find the work function of a field emitter is called the **Fowler-Nordheim Plot**. Using this technique, $\ln(\frac{I}{V^2})$ is plotted over $(\frac{I}{V})$, where the electric field is transferred into a voltage using the relation F=c.V and the emission current density is transferred into an intensity via J=s.I. The linear function coming up from this relation has a slope which is given by the following relation:

$$slope \propto -\frac{1}{\beta}.\phi^{\frac{3}{2}} \tag{2.21}$$

where β is the field enhancement factor and ϕ is the work function of the metal.

Chapter 3

Experimental Setup

3.1 Chambers

In order to do our experiments we need an UHV environment. Two chambers were available in our lab to achieve this condition. Experiments for this thesis were done only in the so called molecule chamber, due to time constraints.

The molecule chamber, is built using standard CF components, and contains a self designed sample holder and cooling system. Pic. 3.1a shows the whole setup, while the sample holder with the cooling mechanism is shown in Pic. 3.1b, but without the sample. In Pic. 3.1c the sample has been installed. The schematic detailed top view of the chamber can be seen in Fig. 3.2 where all necessary components are illustrated.

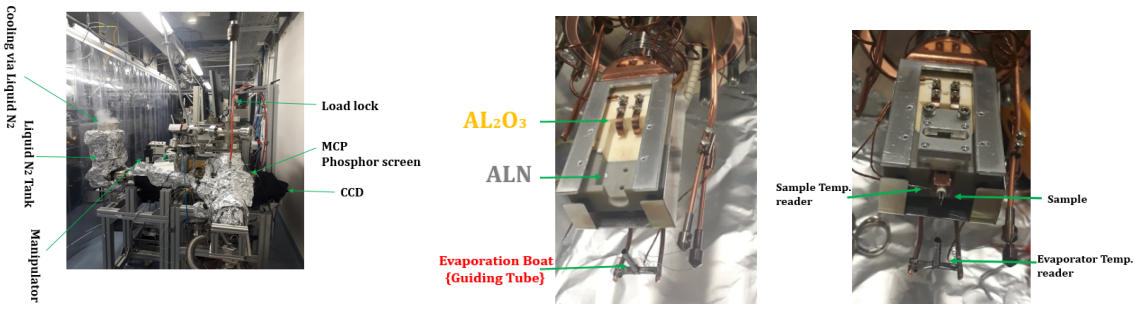

(a) (b) (c)

Figure 3.1: Pictures for our setup; (a) total setup of our molecule chamber labeled with most important parts; (b) sample holder surrounded with the cooling stuff, sample not installed yet, (c) sample has been installed.

The centered white area contains the tip and the cooling mechanism, are the main part of interest to us in this work. It is illustrated in the detailed schematic diagram shown in Fig. 3.3. The chamber was initially pumped using the pre-vacuum pump made by PFEIFFER VACUUM down to 10^{-3} mbar, and then it was bumped using the Leybold TURBOVAC 350i bump to achieve the UHV condition of $1.0*10^{-10}$ mbar.
Now, let's move into the detailed description of the inner components of the chamber.

The sample holder is mounted onto a movable three directional manipulator controlled by a computer through stepper motors. It consists of two parts. The first

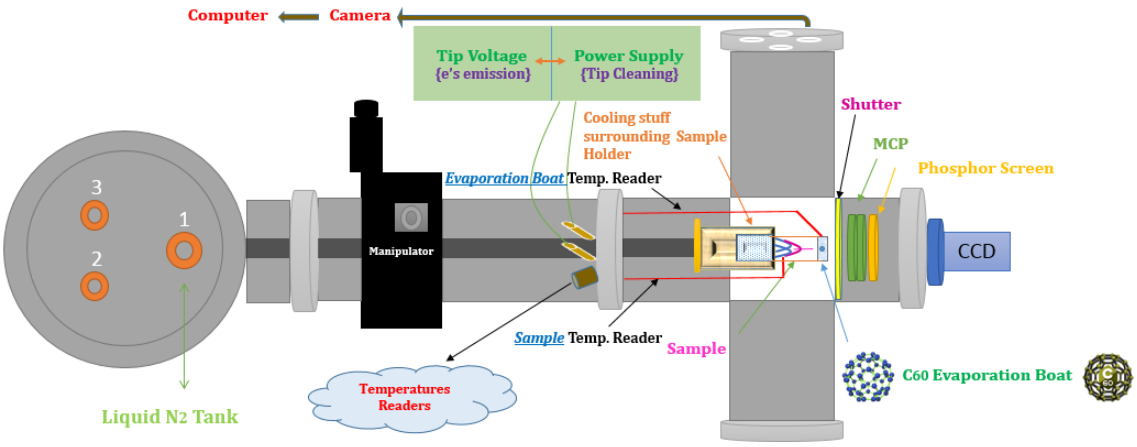

Figure 3.2: Schematic diagram of the top view of our setup

part is mounted onto the manipulator, and a thermocouple is inserted in between the two subparts of this part to read the temperature of the sample. The sample holder can be removed easily through the load lock. This makes tip exchange very fast and easy. This load lock has its own UHV pump such that once the tip is dragged into it, the vacuum inside this load can be broken separately, keeping the vacuum in the main part of the chamber. However, in my experiments, the sample holder was surrounded by the cooling mechanism. This meant that we could not use the load lock to exchange tips, and we had to open the chamber.

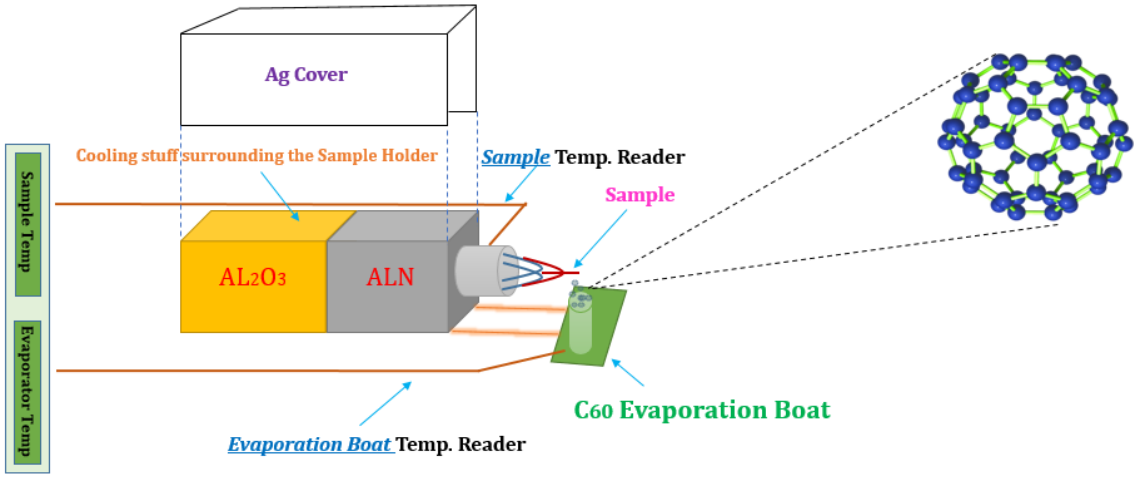

Figure 3.3: A detailed Schematic diagram of the main part of the molecule chamber showing mainly the evaporation boat and the cooling stuff

Cooling the tip was one of the main objectives of our experiments. Liquid nitrogen could reach into a specific point inside the chamber. The plan first was to use a piece made from Aluminum Nitride ALN in order to transport heat carried by the liquid nitrogen out of the sample. However, not enough ALN was available, and we had to attach another piece made from Aluminum Oxide AL_2O_3. There are some advantages of using ALN and AL_2O_3. The high thermal conductivity of these materials guarantees the heat transfer out of sample. ALN, for example, decomposes at $\sim$1800 C^o and this is a significant property, since when we bake the chamber the final temperature is about 160 C^o and we need such a very important chemical sta-

bility. Another crucial feature is the very small thermal expansion coefficient which is important to make sure that components surrounding the sample will hold their shapes and dimensions during temperature changes while cooling the tip.

The C_{60} evaporation system is made from folding a sheet of tantalum. A small hole was then perforated at the centre of this resultant tube to allow C_{60} molecules to evaporate through. However, to protect other components inside the chamber and avoid polluting them, a guiding tube also made from tantalum was attached exactly at the hole so that C_{60} molecules evaporate through it into the tip which is about 1.5 cm above the center of the top part of this guiding tube. After that, this system was spot welded onto two copper electrodes which in turn were connected outside the chamber with a power supply to evaporate C_{60} molecules with controlled amounts through resistively heating the boat. Another thermocouple was spot welded onto the tantalum sheet to read this evaporation boat temperature. Even this is not exactly the C_{60} molecules temperature, since it reads the outer temperature of the boat and not the inner one where C_{60} molecules exist. However, it gives a very precise indication about the evaporation temperature of C_{60} and provides an easy and reproducible way to deposit C_{60}.

Our main challenge was providing a clean environment through cleaning all components inside the chamber to get rid of contamination in order to be able to do such kind of experiments. However, since as I mentioned earlier we could not use the load lock due to cooling stuff, once we had to exchange tip we had to open the chamber from the sample side. Then, ethanol was used to check if there is a leak from that side by squeezing it inside three holes at the joining part and monitoring the vacuum pressure monitor at the computer screen. Now moving into the most complicated part, which is wrapping the chamber with tap heaters and covering it with aluminum sheets to heat up all parts of the chamber. We used to bake it at the end of the week and leave it for two or three days until we reach the saturation point. Where once we start baking, the rate of molecules evaporation from all components inside the chamber and from its internal surfaces is faster than the evacuating pumping speed, so we can see a jump in vacuum monitor program through the computer screen. Then, at some point these two speeds reach a matching point at a chamber temperature of 160 C^o. At this saturation point we stopped baking.

To detect the field emission from tip, a voltage difference is applied between the negatively biased tip and the ground, where the two electrodes of the tip are connected outside the chamber with a power supply which can give voltages up to 5kV. In order to detect as small a number of electrons as possible, two MCP's were installed in front of the phosphor screen and the CCD camera respectively to amplify the number of electrons emitted from the tip. The MCP facing the tip is grounded and the other facing the phosphor screen is positively biased. The amplified emerging electrons from the MCP's were attracted by the anodic, positively biased, phosphor screen which in turn converted them to photons, to be detected by the CCD camera.

Another chamber called, the main chamber, was also available for additional experiments. Initially, Prof. Dr. Michael Altman was here to do a common project with Dr. Yanagisawa, and they wanted to use this chamber for electrons spin detec-

tion. Where Prof. Altman brought with him a spin detector. I could make for them a very beautiful single tungsten tip W100 with an aspect ratio 1:1. This chamber has also an energy analyser that can be used for farther important investigations.

3.2 Electrochemical Etching of Tips for Field Emission Microscopy

Field emission microscopy FEM is based on the phenomenon of electron tunneling through the deformed potential barrier at the metal surface(nanotip). It turns out that well sharpened tips are essential to proceed in FEM experiments in order to study the atomic structure of the tip metal.

FEM tips are usually fabricated from metal wires of tungsten (W) as in our case, and sharpened by a fast, easy, reproducible, reliable manner [23, 24] and cheap method called the electrochemical etching. A picture of the etching machine used in our experiments is shown in Fig. 3.4a and schematically represented in Fig. 3.4b. with a detailed electronic control circuit shown in [25].

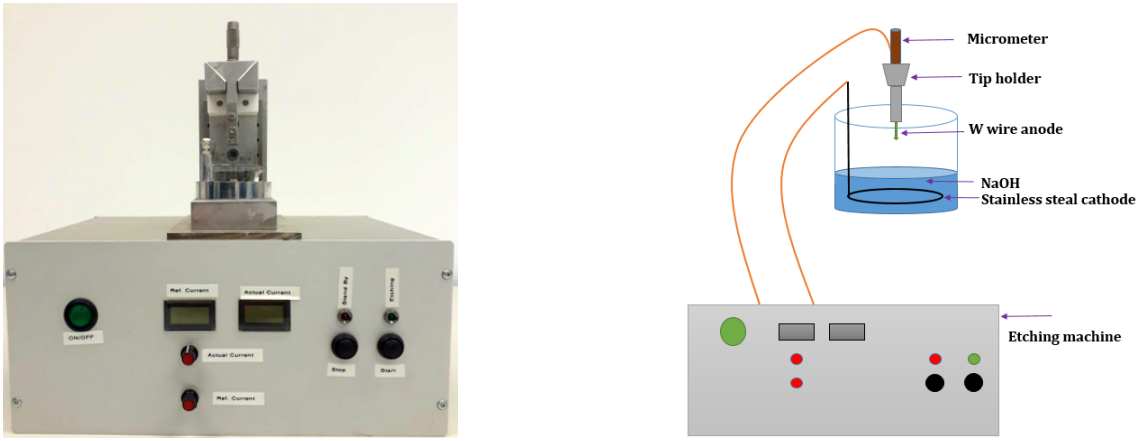

(a) (b)

Figure 3.4: Etching machine (a); with the schematic diagram shown in (b).

Before talking in detail about the etching process, a picture of the spotting machine shown in Fig. 3.5a was used to prepare the tip for etching. Two tungsten wires of lengths 12mm and 4mm were cut and cleaned using glass paper; see Fig. 3.5b. The first was titled from middle to form an arc to carry the tip and was spotted to the tip carrier using the spotting machine. While the second piece was spotted to the loop ,already fixed, to form a spear as shown in the schematic Fig.3.5c.

The electrochemical cell consists of a beaker containing approximately 18ml of 5M NaOH. The W wire which is the anodic electrode in this circuit is placed at the center of the cell, and is mounted on a micrometer to adjust its position relative to the electrolyte surface. The cathodic electrode on the other hand is made from a piece of stainless steel of 1mm thickness and 15mm radius that is circularly bent to fit inside the beaker around the W wire.

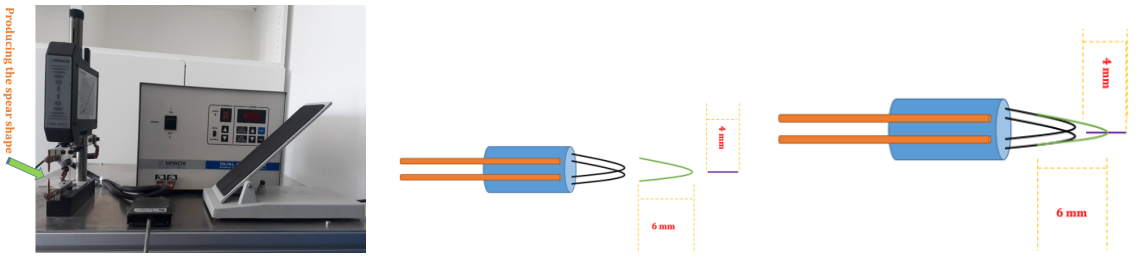

(a) (b) (c)

Figure 3.5: Spotting stages; using spotting machine(a); components to be spot welded(b); and schematic representation of the final outcome(c)

Fig. 3.6a shows a schematic diagram of the electrochemical cell, while Fig. 3.6b shows a schematic representation of the etching process over time.

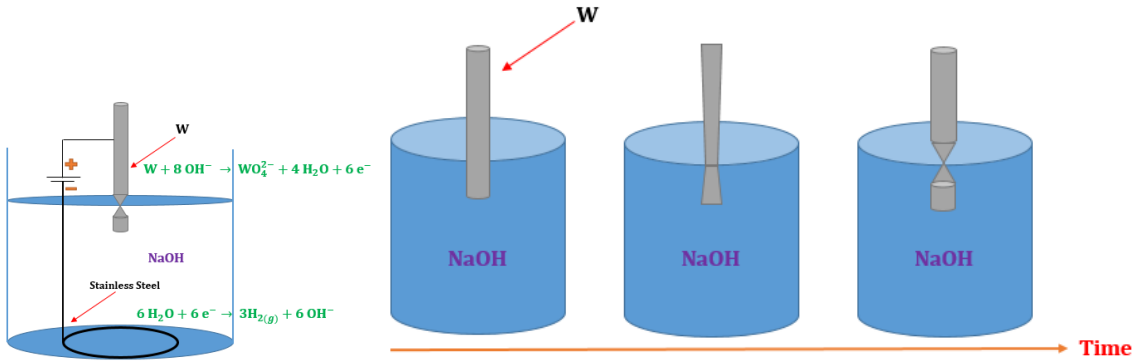

(a) (b)

Figure 3.6: Schematic diagram showing the etching technique; (a) Electrochemical cell of the process; (b) representation of etching over time

When a tungsten wire is immersed in a 5M NaOH solution, the etching occurs at the air-electrolyte interface when a positive voltage is applied to the W wire. The chemical reactions illustrating the process are shown in Fig. 3.6a [25]. During the etch, more parts from the W wire will be etched into the solution. Decrease in the cross sectional area of the wire at that point increases the cell electrical resistance and decreases the cell current respectively. At the etching point, the wire is subject to two forces: the W wire tail weight beneath the etching point pulling the wire downward, and the wire pulling the tail up. As long as the weight does not exceed the tensile strength of the etching point, the tail will still be attached to the wire. However, if the wire cannot take over this pulling down force, the tail breaks and the etching machine records that etching current at a set etching voltage and stops the etching process by shutting down the current supply. Hence, we have two tips simultaneously:the one flows into the solution and the part above the air electrolyte interface which we used. Immediately after finishing the etching the wire was removed and immersed in deionized water to stop any possible remaining chemical reactions. After that, the tip was checked using an optical microscope.

These kinds of tips produced using this method are called dc etched tips. In this experiment I have examined a number of parameters, etching voltage, W wire conditions cleaned or not, and the depth of the W wire immersed within the basic NaOH solution. Each one of these experiments was done at least 3 times. Based on

my observations, I could find the most suitable conditions for the setup used by Dr. Yanagisawa:

1) using an etching voltage of 8.5V and a 1 mm of W immersed in NaOH solution could give a very beautiful, sharp tips with an approximate aspect ratio (1:1).

2) changing the NaOH solution periodically, one time every 3 hours, was very helpful. This makes sense, as we know that based on the mentioned chemical reactions, OH^- is consumed during the etching process.

After practicing for more than 60 hours on the etching machine, I succeeded to etch two W(100) single crystals, where I installed one of them in the main chamber before my leave.

3.3 Principal Techniques Used in Our Experiments

In our experiments there were essential methods used to achieve specific goals. Some were repeated daily, e.g. depositing C_{60} molecules and cooling the tip, while others, e.g. cleaning the tip were done whenever we had to exchange tip, where we had to do this three times. In this section I will explain these methods in detail.

3.3.1 Tip Cleaning in UHV

A well shaped tungsten tip based on our observation using an optical microscope is used inside the molecule chamber of our UHV system. Naturally, the tip surface is covered with contaminants that cannot be easily removed by just rinsing in water, ethanol or acetone.

During electrochemical etching a few nanometers thick of oxide layer [26, 27, 28], mainly tungsten trioxide WO_3 develops on the tip shank [27, 29]. Other contaminants like carbon and microcrystals such as WO_3K also remain over the tip due to etching and exposure to atmosphere [30, 31].

Heating at high temperatures is an effective method adopted in our experiments to clean the tip and desorb contaminants. Two heating steps were used:

1) Tip annealing up to $\sim$ 400 ^{o}C. Fig. 3.2 shows a camera mounted on one of the windows of one of the sides of the chamber which in turn was connected to a computer such that we can monitor the tip while increasing the heating power gradually until we reach a point where the tip starts to glow. Then, we anneal it for $\sim$ 30 minutes and stop annealing for 30 minutes, and this cycle is repeated 5 times.

2) Tip flashing where we heat the tip up to $\sim$ 800 ^{o}C. As one can tell from the name, we increase the tip temperature for $\sim$ one second and make sets of such heating pulses. We start this step from the annealing power, and repeat such pulses until we notice a quick pressure recovery after finishing each set of these pulses. This process is repeated while moving up in the heating power gradually. We can

imagine this as removing one layer of contamination at each heating power, then moving down into a deeper contamination layers.

It has been reported that when the heating temperature exceeds 1000K, the oxide layer of WO_3 covering the tip reacts with the tungsten to produce the volatile tungsten dioxide WO_2 which leaves the metallic tip clean. This is summarised in the following reaction [32]:

$$2WO_3 + W \longrightarrow WO_2 \uparrow_{volatile}$$

Hence, the aim from the flashing process is to reach a temperature high enough to remove the oxide layer, but not too high, to avoid a significant tip blunting. Besides this, it helps to heal the defects caused by the electrochemical etching [33, 34] and smooths the tip surface to reach the atomic structure of the clean tungsten surface.

The final shape of the tip after successfully passing through the cleaning procedures is determined by two operations:
1) evaporation of atoms from its surface which sharpens the tip apex.
2) diffusion of atoms from the tip apex towards the tip shank which increases the apex radius of curvature [34].
However, diffusion effect dominates the evaporation effect as the latter happens at very high temperatures [35].

3.3.2 C_{60} Deposition Mechanism

The method used to deposit C_{60} molecules was through a self designed setup shown and well explained in detail in Fig. 3.3. By using a timer and knowing the reading of the outside surface of the evaporation boat through the thermocouple, we adjust the heating power to deposit C_{60} molecules at the desired temperature as long as we want. Mostly, I used to deposit for 15 minutes. However, it is not so easy to deposit for long time at the same temperature as it increases suddenly, so I had to keep adjusting the heating power. We also used to deposit C_{60} at different evaporation temperatures with 10 degrees steps, since based on my experience there was an error in the deposition temperature of nearly ± 2 ^{o}C. In section 4.3 I will talk in detail about a long experiment we did to find a relation between the number of C_{60} molecules deposited and the evaporation temperature.

3.3.3 Tip Cooling Method

The cooling system was built in our lab. By checking Fig. 3.2 starting from the left side of our setup, we see the liquid nitrogen tank where we add liquid N_2 gradually through entrance (1). Outlets (2,3) are designed to allow air bubbles to go out the tank while replacing it with the liquid N_2. Typically I needed 20 minutes to fill the tank. The nitrogen then goes through a stainless steel cylinder with variable diameter where the very end point has a diameter of 16mm, and has a copper cover. This cover is attached to a piece of Aluminum Oxide AL_2O_3 which is also attached to another piece of Aluminum Nitride ALN where these two very hard conductors

couple the liquid N_2 to the tip to cool it down. Based on my observations, after filling the tank, the tip needs one hour to be cooled from the room temperature to $\sim$ -180 ^{o}C.

Chapter 4

Investigations of FE Over the Tungsten Surface (First Reference Surface)

This chapter is the starting point of our experiments. The first section will explain the stages of the tip cleaning process. In the second section, we looked through the FEM on a low and high C_{60}-covered tip, while we clarified the relation between the deposition temperature and the amount of C_{60} molecules deposited in the third section. In the fourth section, we could also observe through the FEM how stable the deposited C_{60} molecules onto the **cooled** nano-tip are in both the low and high coverage regimes, and in the last section we did an experiment to show the effect of contamination on the FE and how this limits the available time for experiments.

4.1 Obtaining the Clean Tungsten Surface

A reproducible starting point in such kind of experiments is of great significant. A successfully produced etched tip is not clean as it is initially completely covered with contaminants from the etching process and exposure to air. In order to remove this contamination from the surface of the tip, a cleaning technique, which I clarified in detail in sec. 3.3, is adopted. Fig. 4.1 shows the change in FE pattern while cleaning the tip, where only one spot appears in picture 4.1a which means that the tip is completely contaminated and this layer of contaminants acts as a barrier preventing us from seeing the FE from the tip. While cooling we can see a more symmetric pattern start to appear until we get a well recognized clean tungsten surface [12, 14, 36, 37] as it is shown in picture 4.2a.

Once we have our reference starting point clean W surface we deposit C_{60} molecules and determine the heating power necessary to clean the tip by gradually increasing the heating power while the tip is covered by C_{60} molecules, where each flashing corresponds to a deposition process.

The final pattern is a work function map of the tip apex [18, 19] as we can see in Fig. 4.2, where picture 4.2a is the FEM of the actual clean tungsten surface, and picture 4.2b is for the clean tip apex. The lower the work function is, the more emitted electrons; and hence the most intense emission spot is observed around the

(310) crystal facets which has the lowest work function. However, the relatively high work functions of the (011) and (010) crystal faces [38, 39, 40] suppress the intensity of field emission from these regions.

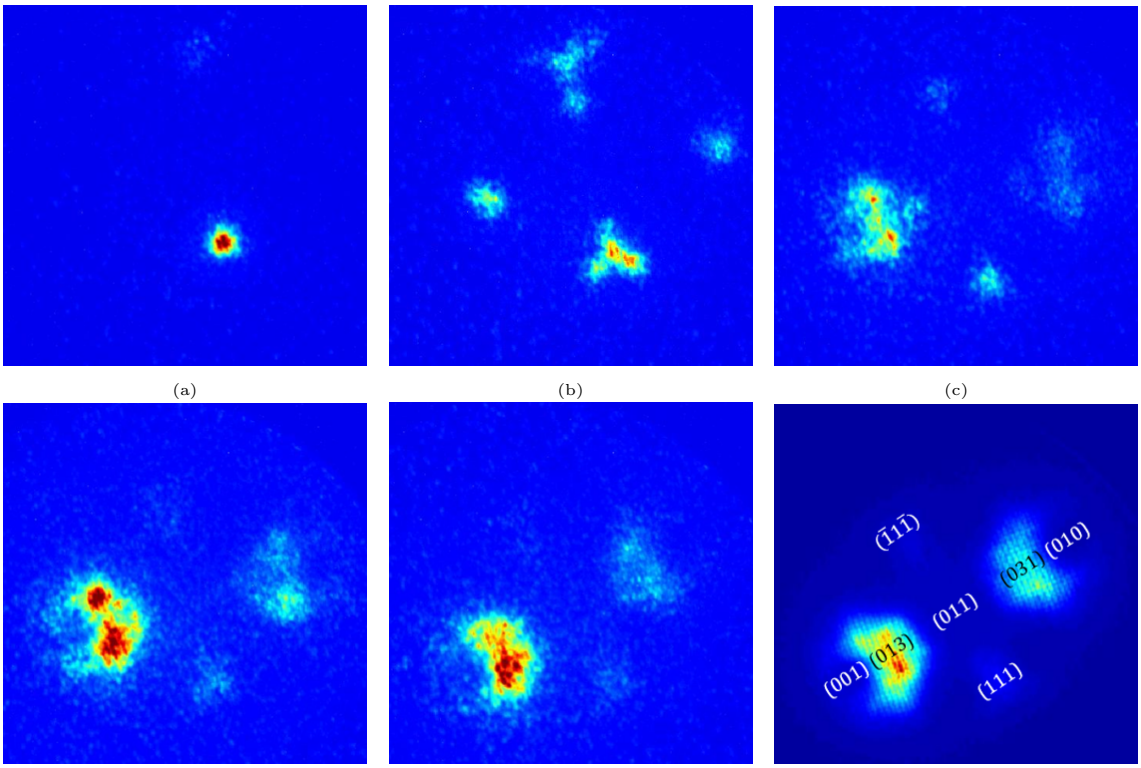

Figure 4.1: FEM pictures showing the smooth symmetric transformation of the FE from a tip at different stages during it's cleaning journey. Blue and read colors indicate a low and high FE intensity respectively, while dark red color represents a regions where the CCD camera has been saturated.

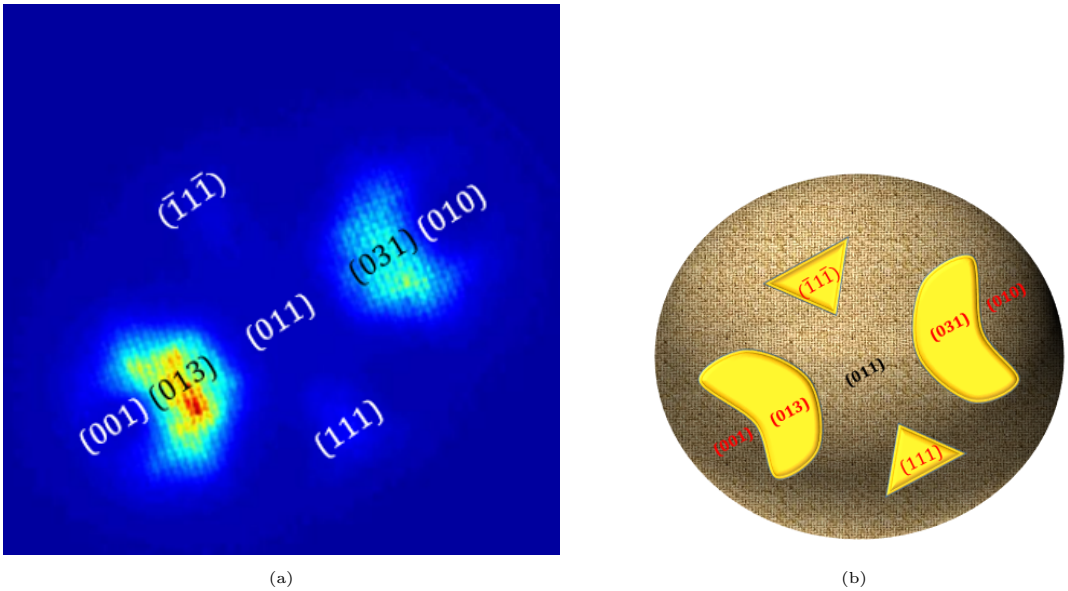

Figure 4.2: Work function map of the tip apex with; (a) FEM of the actual clean tungsten surface; (b) my model of the tip apex with its work function map.

During this work, I cleaned two tips. Based on my experience, the time needed to finish cleaning differs based on how clean the tip is once installed in the chamber.

The first tip was already in the chamber, and I needed roughly 90 hours to clean it. However, for the second tip one I made myself, I needed about 10 hours. This of course depends on the etching process mainly, and other factors before it is installed in the chamber.

4.2 Impact of Different Deposition Conditions on Observed Structures

Now, by obtaining the clean tungsten surface, the next step is to deposit C_{60} molecules. In this section I will describe the general deposition behaviour based on different deposition conditions. First I will characterize the pattern of field emission from a tip covered with a little amount of C_{60} molecules. Afterwards, I will move into a thicker layer deposition behaviour. In the next section I will support this by an experiment linking the deposition condition with the FEM pattern.

4.2.1 FEM on Low C_{60}-Covered Tip

As we now have our reproducible starting point illustrated in the previous section, we can deposit C_{60} molecules over the tip. In this section I am going to show the FE behaviour while the tip is covered with a little amount of C_{60} molecules.

In fact we do not have a device to measure exactly the amount of C_{60} deposited. However, our method explained in section 3.3.2 is a well controllable and reproducible technique that can be used to deposit C_{60} molecules as much as we desire. The variables during the deposition process are the deposition time and the evaporation deposition temperature which in turn can be controlled by adjusting the heating power.

A low C_{60}-covered tip means features of the original clean tungsten surface are still visible. It is assumed that the small circular spotted structures pattern appearing after deposition indicate the presence of C_{60} molecules. Even though it is not clear if these refer to single C_{60} or clusters of them. Similar features were observed in [41].

Typically, below 240 ^{o}C deposition temperature I could not see an emission corresponding to C_{60} emission. However, roughly between 250 ^{o}C and 360 ^{o}C deposition temperatures I still could see an emission from the tungsten substrate. At higher evaporation temperatures as I will show in the next section the substrate becomes totally covered and we will see a field emission only from the C_{60} molecules covering it. In section 4.3 I will illustrate this point. Nevertheless, these deposition temperatures are not fixed, as an example if we open the chamber to exchange the tip, the position of the new tip may not be the same as the previous one and hence the amount of C_{60} molecules deposited over each tip differs based on its position with respect to the evaporation boat.

To clarify the idea, Fig. 4.3 demonstrates the previous discussion. The upper panel shows FEM pictures taken for a clean tip surface, after depositing C_{60}

molecules, and after cleaning the tip by flash heating it starting from left to right respectively. The middle FEM picture of the upper panel corresponds to C_{60} deposition at **220** ^oC for **5** minutes with 500 voltages negatively biased tip. The lower panel is my model for this deposition behaviour.

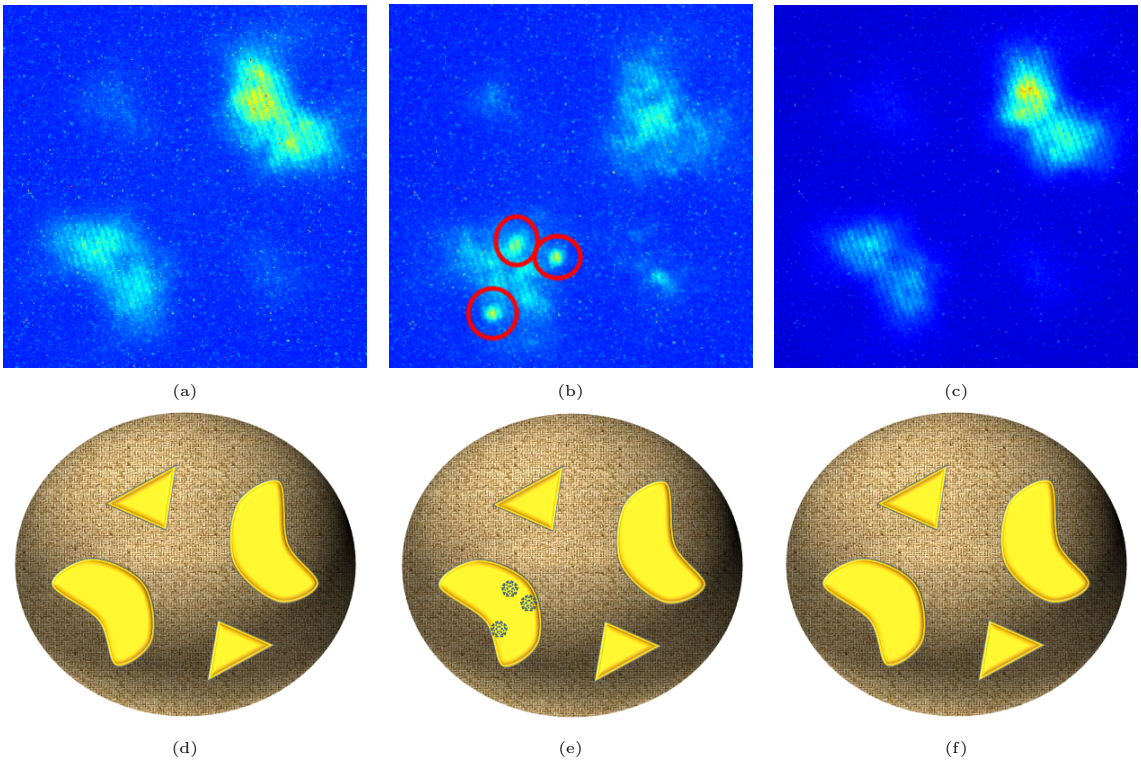

Figure 4.3: Field emission behaviour at low deposition temperature. The upper panel is:(a) FEM picture of a clean tungsten tip; (b) FEM from a tip after C_{60} deposition at **220** ^oC for 5 minutes; (c) FEM after flashing the tip. The lower panel is the corresponding tip apex ball model.

From Fig. 4.3 we can see three spotted features appeared at the **lower part of the tip** (corresponding to C_{60} molecules) and a field enhancement is noticeable at their positions compared to neighboring areas. Actually, C_{60} molecules are randomly deposited all over the tip, but wherever the work function is low enough such that the voltage is high enough to trigger FE from C_{60} molecules. This matches the theoretical discussion in sections 2.4 and 2.5.

In the next section I will deposit at high evaporation temperatures and discuss the pattern of field emission.

4.2.2 FEM on High C_{60}-Covered Tip

In the previous section I showed how the FEM looks if we deposit a little amount of C_{60} molecules over the tip. We could easily still distinguish the field emission from the substrate itself compared to that due to the C_{60} molecules.

In this section I deposited more C_{60} molecules such that we can hardly see the emission from the substrate, where it is completely covered with C_{60} molecules and the emission we observe is mainly from the C_{60} molecules as we can see from Fig.

4.4a. My model for this deposition behaviour is shown in Fig. 4.4b where mainly C_{60} molecules gather on the most intense faces of the substrate.

In this figure I evaporated C_{60} molecules at **370** ^{o}C for **15** minutes with 500 voltages negatively biased tip. Many spots refer to C_{60} molecules are observed. At this deposition temperature, most likely, the tip is covered with C_{60} molecules and even some of them form pyramids if more that one monolayer is deposited.

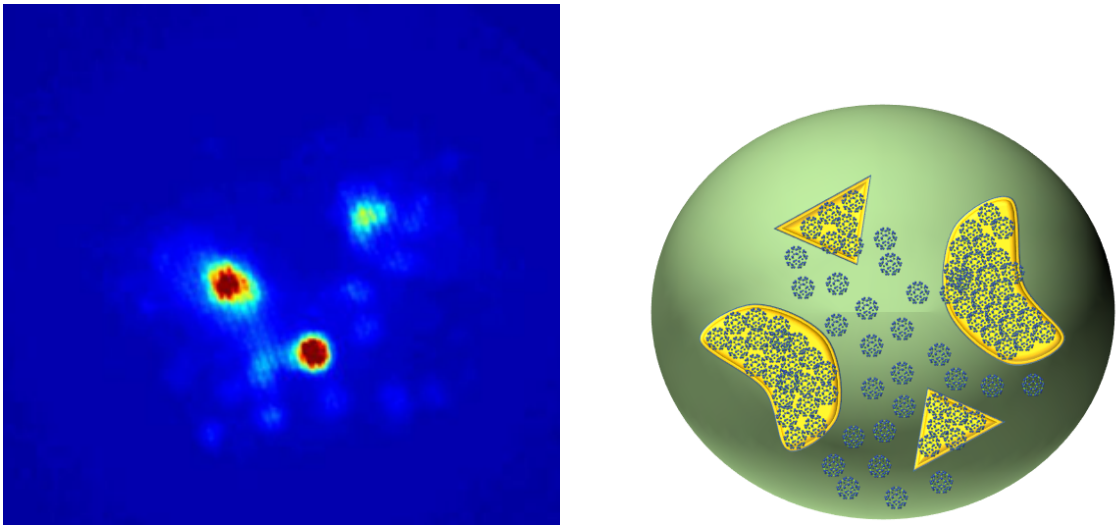

(a) (b)

Figure 4.4: Field emission behaviour at high deposition temperature. (a) FEM from a tip after C_{60} deposition at **370** C^{o} for 15 minutes; (b) My tip apex ball model for this deposition behaviour.

4.3 Relation between amount of C_{60} molecules and evaporation temperature

In sections 4.2.1 and 4.2.2 I gave a general deposition behavior at low and high deposition temperatures. To illuminate this point we did a lengthy experiment ($\sim$ one month). The aim was to confirm that the spots we detect after deposition originate from C_{60} molecules. One would expect an increase in the number of spots as the evaporation temperature increases.

To achieve this goal we cooled the tip using liquid nitrogen down to $\sim$-180 ^{o}C, since at this very low temperatures, we get better vacuum compared to room temperature. This should decrease the probability that these spots are due to other contaminants existing within the chamber. The cooling process is explained in section 3.3.3. In chapter 5, I will talk in more details about tip cooling.

Once the tip was cooled, I deposited C_{60} molecules at different evaporation temperatures starting from **370** ^{o}**C** and went down to **260** ^{o}**C** with **10** ^{o}C degrees step. At each deposition temperature the experiment was done three times, where each time I deposited for **15** minutes with 500 voltages negatively biased tip. We could observe a qualitative decrease in the number of spots while decreasing the evaporation temperature. We also noticed an exponential relation between the evaporation

temperature and the number of C_{60} molecules evaporated as it is shown in [42, 43]. One can state that it is not so easy to calibrate the amount deposited. Fig. 4.5 elucidates this confirmational experiment.

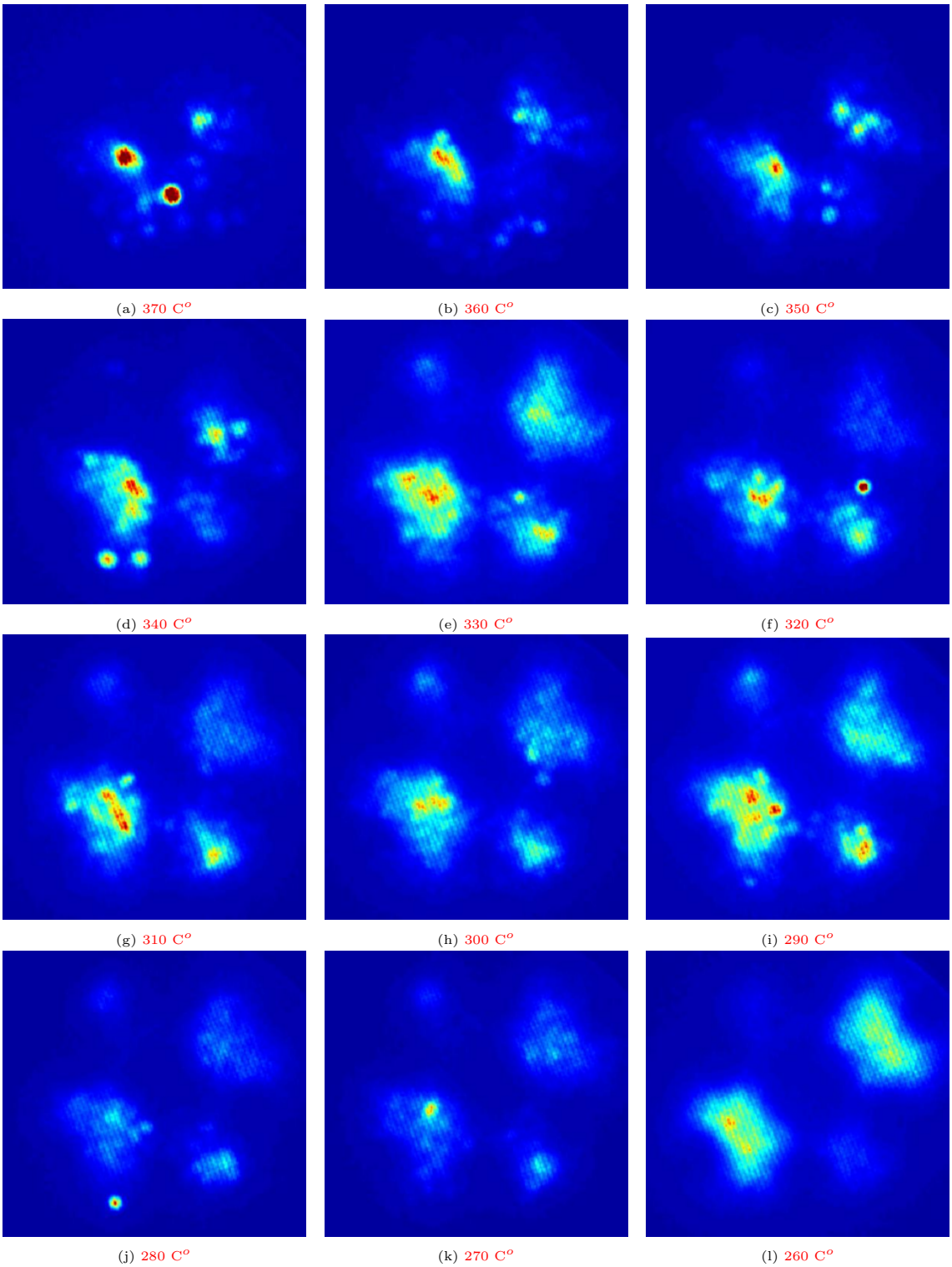

(a) 370 C^o (b) 360 C^o (c) 350 C^o

(d) 340 C^o (e) 330 C^o (f) 320 C^o

(g) 310 C^o (h) 300 C^o (i) 290 C^o

(j) 280 C^o (k) 270 C^o (l) 260 C^o

Figure 4.5: FEM pictures from a C_{60}-covered tip at different coverage regions corresponding to different evaporation temperatures. Deposition temperature is labeled for each FEM.

To explain this experiment I will use my simple ball model for the tip apex. In the model shown in Fig. 4.6 there is a dotted black line to separate the upper and

lower parts of the tip apex, and a continuous red circular line joining the upper to yellow areas representing the two sets of facets (031) and $(\bar{1}1\bar{1})$.

The first FEM picture taken after depositing at 370 ^{o}C represents a completely covered tip apex as we can not see the substrate. At 330 ^{o}C we somehow start to distinguish the yellow areas of the substrate represented by my model. At 310 ^{o}C the two sets of facets included by the red line of my model are easily distinguishable and there are no spots corresponding to C_{60} molecules . However, we still can see many spots on the lower part of the tip apex under the black dotted line of my model. This matches our expectations as it is the part of the tip exposed to the evaporation boat. By decreasing the evaporation temperatures the number of these spots even at the lower part of the tip apex decreases as one can see from the two FEM pictures 280 ^{o}C and 270 ^{o}C. Finally, at 260 ^{o}C we are back again to the clean tungsten surface.

So, based on these observations:

- The number of spots decreases with decreasing evaporation temperatures.
- At lower evaporation temperatures we mainly see spots on the lower part of the tip apex under the black dotted line of my model for the tip apex, and rarely see such spots on the regions included by the red circular line of my model.

These observations strongly support our hypothesis that these spots correspond to C_{60} molecules.

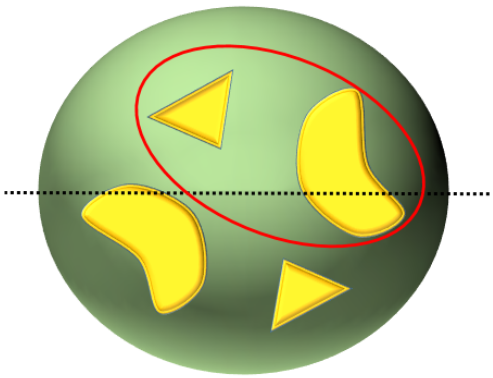

Figure 4.6: Ball model for the tip apex. The black dotted line separates the upper and lower parts of the tip apex; the red circular line includes the upper two sets of facets (031) and $(\bar{1}1\bar{1})$.

4.4 Stability of C_{60} Molecules On the Surface of a Cooled Tip

One of the most interesting features we could observe is the stability of C_{60} molecules deposited over the nano-tip.

In this experiment we cooled the tip using liquid nitrogen down to ~ -180 ^{o}C and deposited C_{60} molecules at different temperatures for **15** minutes with 500 voltages negatively biased tip comprising the low and high coverage regions. I will present two of them: namely the 260 ^{o}C as an example for the low coverage case, and the 370 ^{o}C for the high coverage case. We took a long video to investigate the dynamics and in Fig. 4.7 and Fig. 4.8 I chose some of these FEM pictures each labeled with the time it was recorded at.

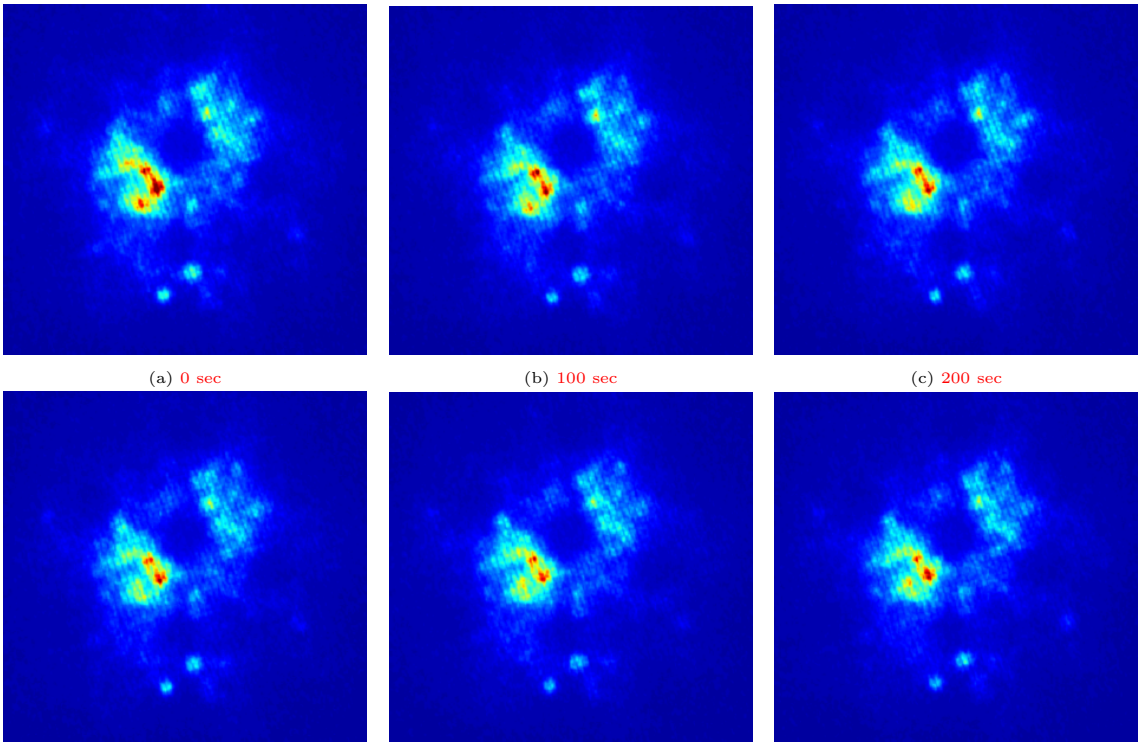

(a) 0 sec (b) 100 sec (c) 200 sec

(d) 300 sec (e) 500 sec (f) 600 sec

Figure 4.7: FEM pictures for a C_{60}-covered tip at 260 ^{o}C deposition temperature for **15** minutes with 500 voltages negatively biased tip; showing the dynamical stability of FE at such low evaporation temperatures.

As we can see, there is no dramatic change in the field emission, with the patterns staying basically stable. This is an important advantage to be used if the tip is illuminated with laser.

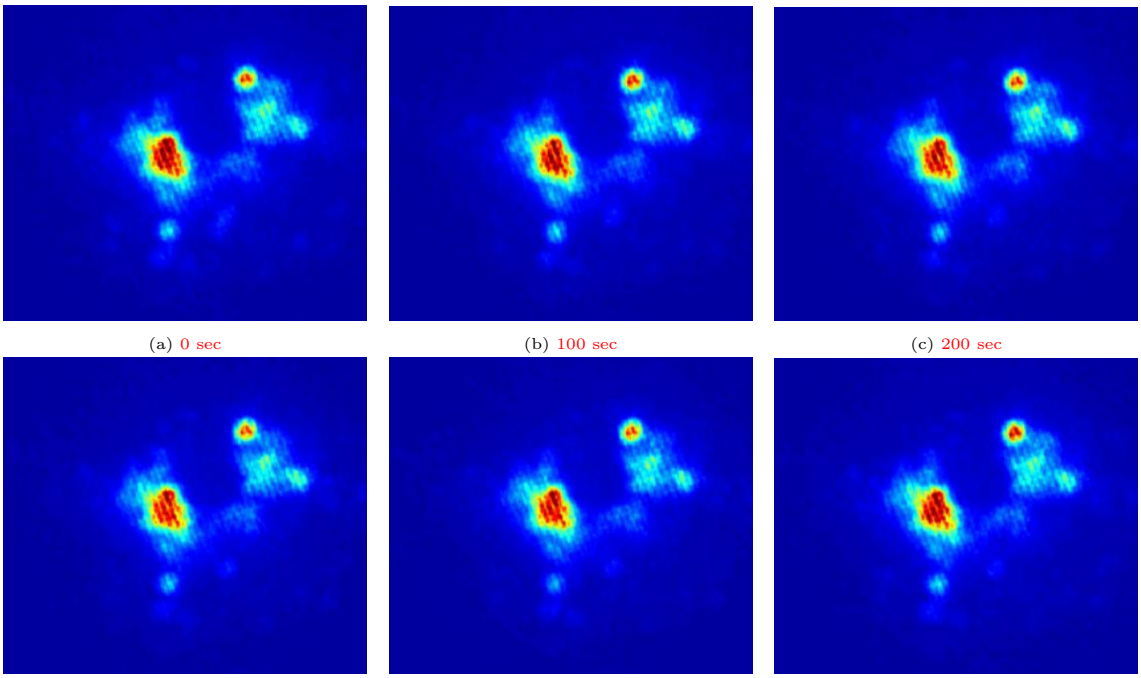

(a) 0 sec (b) 100 sec (c) 200 sec

(d) 300 sec (e) 500 sec (f) 600 sec

Figure 4.8: FEM pictures for a C_{60}-covered tip at 370 ^{o}C deposition temperature for **15** minutes with 500 voltages negatively biased tip; showing the dynamical stability of FE at even such high evaporation temperatures.

4.5 Clean Surface Experiment

Over time, a clean tungsten surface as well as a clean tungsten carbide will be contaminated. This in turn affects emission from the tip and limits the available time for experiments. This should be taken into consideration. To study this phenomenon, we cleaned the tip, then immediately took an FEM. After 30 minutes I then took another FEM. This was repeated 10 times.

We observed a decrease in the intensity of the field emission from the tip over time. Fig. 4.9 clarifies this idea, where the left FEM 4.9a is a picture for a clean surface taken directly after flashing the tip, with a tip voltage of -2440 Volts. The middle FEM in the panel 4.9b is a picture for the tip after 30 minutes waiting with a negatively biased tip of -2600V, while the right FEM 4.9c is for a tip after 30 minutes but with a higher tip voltage of -2660V.

We conclude that intensity of field emission from a contaminated tip left for a while is less compared to that from a freshly cleaned one. The contaminants blocked field emission, and we had to increase the tip voltage to overcome this contamination barrier.

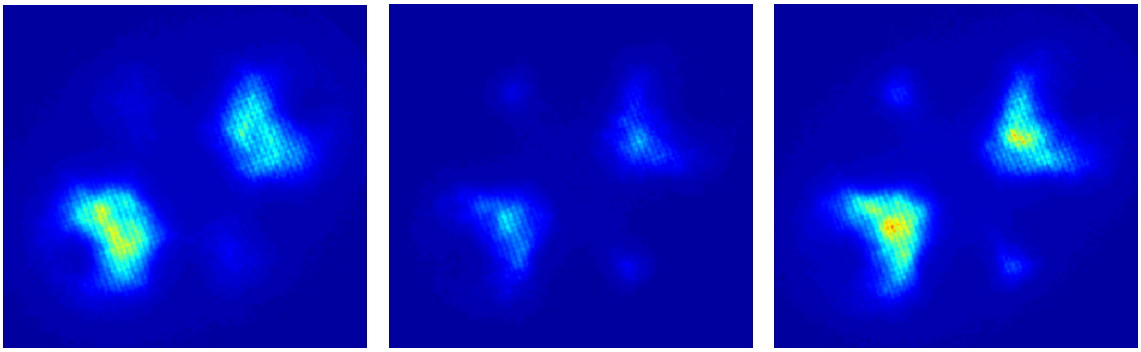

(a) 0 sec(-2440V) (b) after 30 minutes(-2600V) (c) after 30 minutes(-2660V)

Figure 4.9: FEM pictures; (a) clean tungsten surface; (b) after 30 minutes waiting with -2600 volts negatively biased tip; (c) after 30 minutes waiting with -2660 volts negatively biased tip;

Chapter 5

Investigations of FE Over the Tungsten Carbide Surface (Second Reference Surface)

In the previous chapter, I discussed experiments done on the tungsten surface. In this chapter I will discuss similar experiments on tungsten carbide surface, and compare between the two cases. Hence I will start this chapter by explaining the process of getting the tungsten carbide surface. I will also discuss the formation of clover leafs at low deposition temperatures, and determine a direct relation between the tip voltage and the number of clover leafs.

5.1 Formation of Tungsten Carbide

In the previous chapter we saw how the clean tip surface looks like as shown in Fig. 5.1a . In order to keep that surface, we avoid going into a high deposition temperature regime. Otherwise, if the tip is highly covered with C_{60} molecules and flashed to be cleaned, the clean surface will be transformed from the clean tungsten into the clean tungsten carbide surface which has special features as one can see from Fig. 5.1d . The actual reason behind this transformation is not known. However, carbon atoms are needed for this conversion to occur. Chemically, two well-characterized chemical compounds can be produced when tungsten reacts with carbon atoms at high temperatures: tungsten carbide WC, and tungsten semicarbide W_2C. In our case, it might be a combination of both depending mainly on the temperatures used. Flashing the tip at high temperatures decomposes C_{60} molecules [44, 45, 46, 47, 48, 49] covering it and the resulting carbon atoms diffuse into the tungsten metal surface to form the tungsten carbide.

We could notice that the transformation of tungsten surface into the tungsten carbide is not a dramatic form change. Instead, intermediate structures appear before getting the final feature of the tungsten carbide as shown in Fig. 5.1b and Fig. 5.1c.

Now we have our second reference point which is the clean tungsten carbide surface. In fact we can go back to the clean tungsten surface by increasing the heating power to decompose the formed tungsten carbide into tungsten and carbon

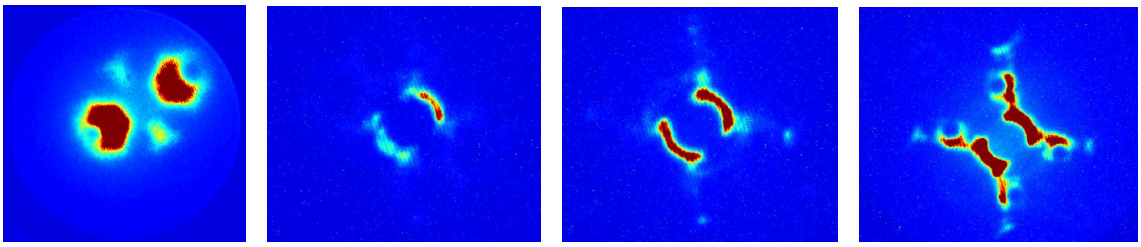

(a) (b) (c) (d)

Figure 5.1: FEM pictures showing the transformation of the clean tungsten surface (a), into the clean tungsten carbide surface (d) with it own unique symmetric pattern; passing through the intermediate structures (b,c). Pictures are normalised to their own highest value. Blue means low intensity areas, while red means high intensity field emission areas.

atoms. However, by increasing the heating power we increase the chance of blunting the tip and eventually we have to replace it. Hence, once we get the tungsten carbide we keep it. In the next section we will discuss depositing C_{60} molecules.

5.2 Impact of Different Deposition Conditions on Observed Structures

In chapter 3 I discussed the influence of C_{60} evaporation at different temperatures onto the tungsten surface. On that surface, all we could detect are circular spots in the low and high coverage regimes. However, in this section I will show very interesting structures that appear when the tip is highly covered with C_{60}. But, before doing that I will show how the pattern looks like in the low coverage regime.

5.2.1 FEM on Low C_{60}-Covered Tip

In section 4.2.1 I discussed the field emission pattern from a tungsten tip covered with a little amount of C_{60} while the clean tungsten surface was our reference point. In this section we have a new reference, namely, the clean tungsten carbide surface. We did a similar set of experiments to that using the clean tungsten surface as our reference. We could also observe spotted structural features mainly on the lower part of the tip. However, we needed mostly higher deposition temperatures to detect these spotted structures. This might be due to a different sticking coefficient when we have the tungsten carbide surface compared to the tungsten surface. Fig. 5.2 shows two FEM pictures taken for a C_{60}-covered tip in the low coverage regimes with orange arrows indicating the plausible positions of C_{60} molecules. Again, by low regimes I mean we still can see features of the substrate, in this case the tungsten carbide surface. As one can see, sometimes it is possible for the tungsten carbide features to rotate from tip to tip, where Fig.5.2a shows a clean tungsten carbide for the first tip, while the rotated tungsten carbide in Fig. 5.2b for the second tip used. Next, I will discuss higher deposition temperatures to investigate the most important part of this research.

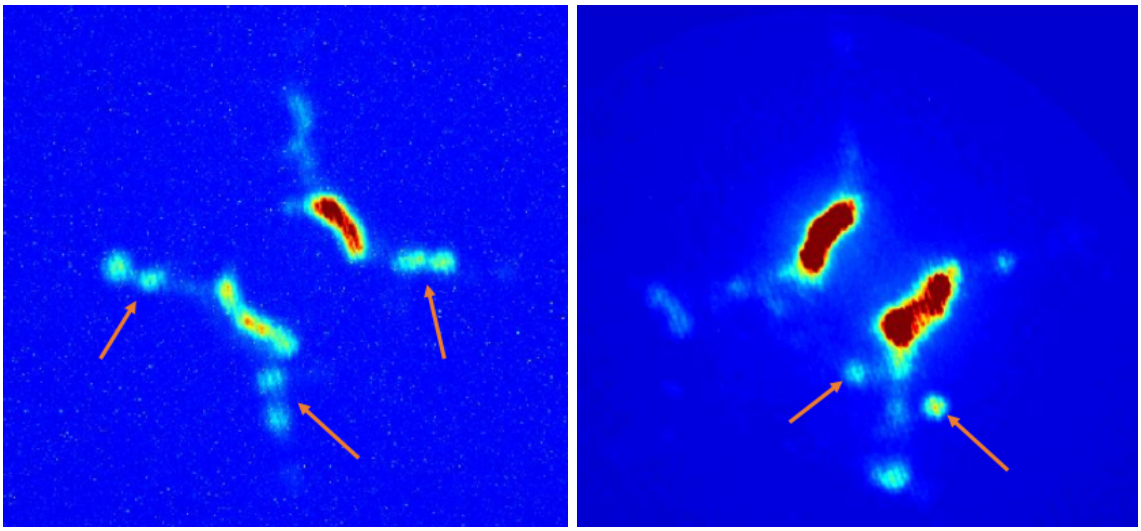

(a) (b)

Figure 5.2: FEM pictures for a low C_{60} covered tip with the orange arrows indicating the possible position of C_{60} molecules. Pictures are normalised to their own highest value. Blue means low intensity areas, while red means high intensity field emission areas

5.2.2 FEM on High C_{60}-Covered Tip

It is time to deposit more C_{60} molecules by increasing the evaporation temperatures. We did this gradually and we could observe the increase in the covered regimes of the tip. At the beginning, we could see the spotted features which I showed in the previous section. Afterwards, the lower part of the tungsten carbide started to disappear gradually until it was completely covered. At this point we are sure that this part of the tip, namely the lower part, is covered at least by one monolayer of C_{60} molecules. Depositing more C_{60} leads to the appearance of distinct features onto the lower part of the tip. At this point the upper part of the substrate could still be seen. This deposition behaviour is shown in Fig. 5.3.

The very interesting feature of the high coverage regime is the appearing of unique spots on the lower part of the tip when it is completely covered with C_{60}. Fig. 5.4 shows some FEM pictures taken at different deposition conditions on different days. This also is an amazing feature where as long as we deposit high amounts of C_{60} molecules we end up with similar patterns no matter what deposition conditions are considered. However the number of these distinct structures will be discussed later. We could observe different structures. However, the most attractive, distinguishable, and interesting patterns are the four-cloverleaf patterns as it is shown in Fig. 5.4c, and the two-cloverleaf patterns shown in Fig. 5.4a. Similar patterns were also observed in [50, 51].

The main purpose of these experiments is to stabilize the FE patterns including the cloverleaf's for farther studies hoping to find out the reason behind the formation of these special features. Historically, when pthalocyanine was deposited over the tip to study field emission they tried to find a relation between the shape of pthalocyanine molecules and the resulting structures [20, 52]. A pthalocyanine molecule has two cases whether standing up onto the tip apex or laying down. In the first configuration it exhibits a 4-symmetric pattern, while in the other configuration it

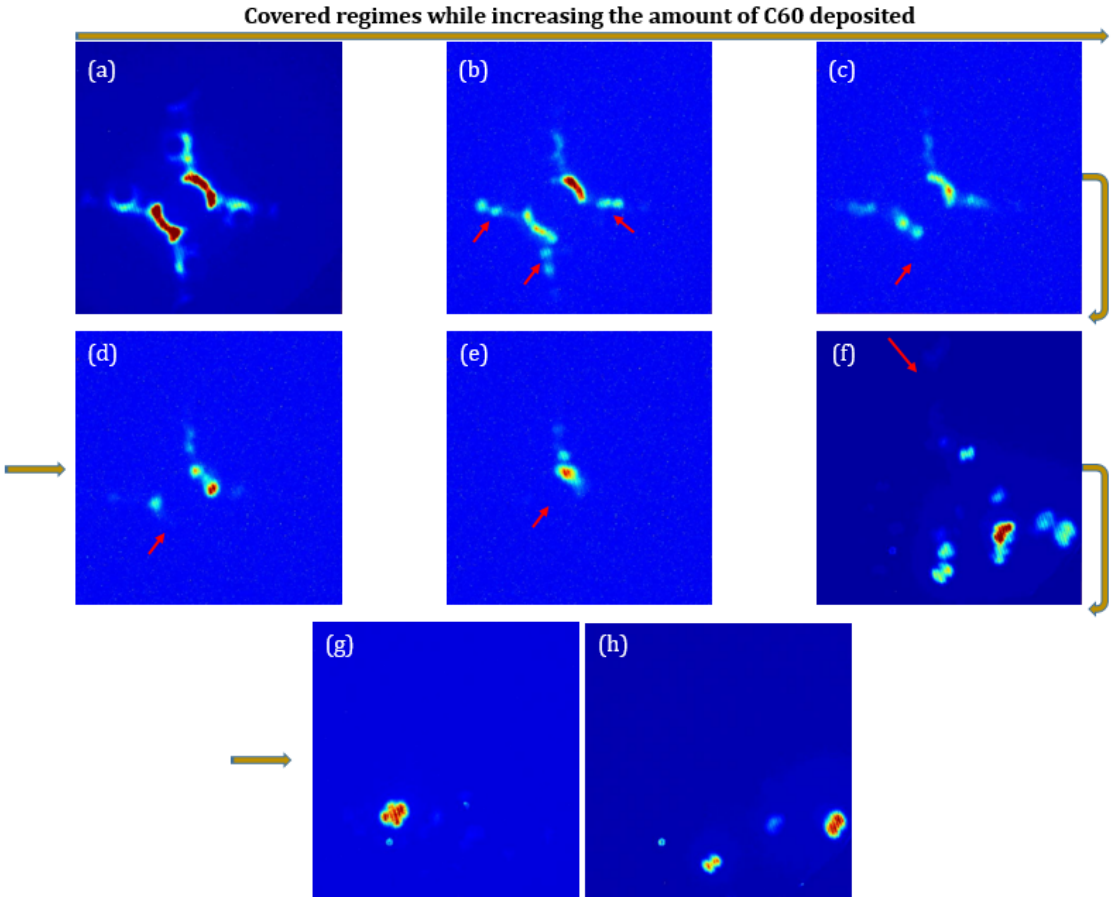

Figure 5.3: FEM pictures for the deposition behaviour while increasing the amount of C_{60} evaporated starting from the clean tungsten carbide surface (a); spotted structures appeared in (b); the lower part of the tungsten carbide started to be covered by increasing the deposition; clover leaves appeared while still the upper part of the tungsten carbide visible (f); then in (g) and (h) the upper part even has been totally covered showing the most important class of these structures (clover leaves). Red arrows indicate appearing of new structures or disappearing parts of the tip. Blue means low intensity, while red indicates high intensity. Pictures are normalised to different values to get best show.

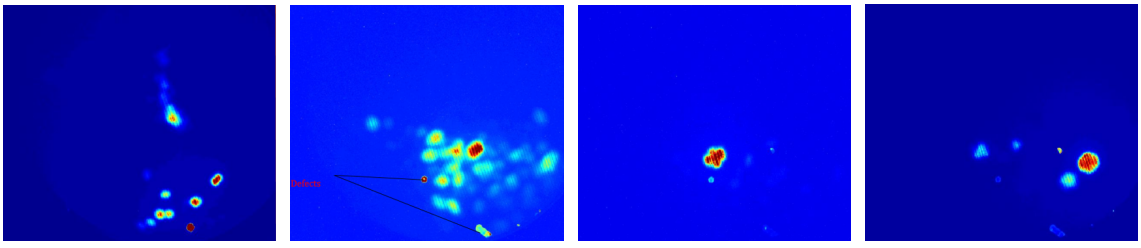

(a) (b) (c) (d)

Figure 5.4: FEM pictures showing the distinct spotted features after covering the tip with a large amount of C_{60}; (a) mainly we can see the two fold symmetry pattern; (c) a very beautiful 4-leaf pattern. Blue regions mean low intensity, red means high intensity. Each picture is normalized to its own highest value.

displays a 2-symmetric pattern. So, they tried to correlate the 2 and 4-cloverleaf patterns with these configurations. Later, they found out that this is not true, where different molecules which do not exhibit neither a 2 or a 4 fold symmetric patterns can come up with these features [53]. Some correlated this with the number of molecules deposited [12]. According to this theory, in our case C_{60} molecules gather to form small clusters having a small number of C_{60} molecules, where the shape of the pattern is related to the number of these molecules forming the corresponding cluster.

However, we believe that the energy levels of each one of the C_{60} molecules is the reason causing this phenomenon. That is, each one of these patterns results from a single C_{60} molecule and not from a cluster of C_{60} molecules. The diversity of patterns in turn is due to the different shapes of the energy orbitals. A C_{60} molecule in the s-state emits electrons which appear as a circular spot on the phosphor screen, while emitted electrons from another C_{60} molecule in the p-state produces a two-fold symmetry pattern on the phosphor screen. The most important pattern, namely the 4-clover leaf, results in turn from a C_{60} molecule occupying the d-state energy level, and so on. Fig.5.5 summarises the whole story, where the middle panel shows the energy levels models for the s,p and d-states, and their actual shape appearing on the phosphor screen in the lower panel.

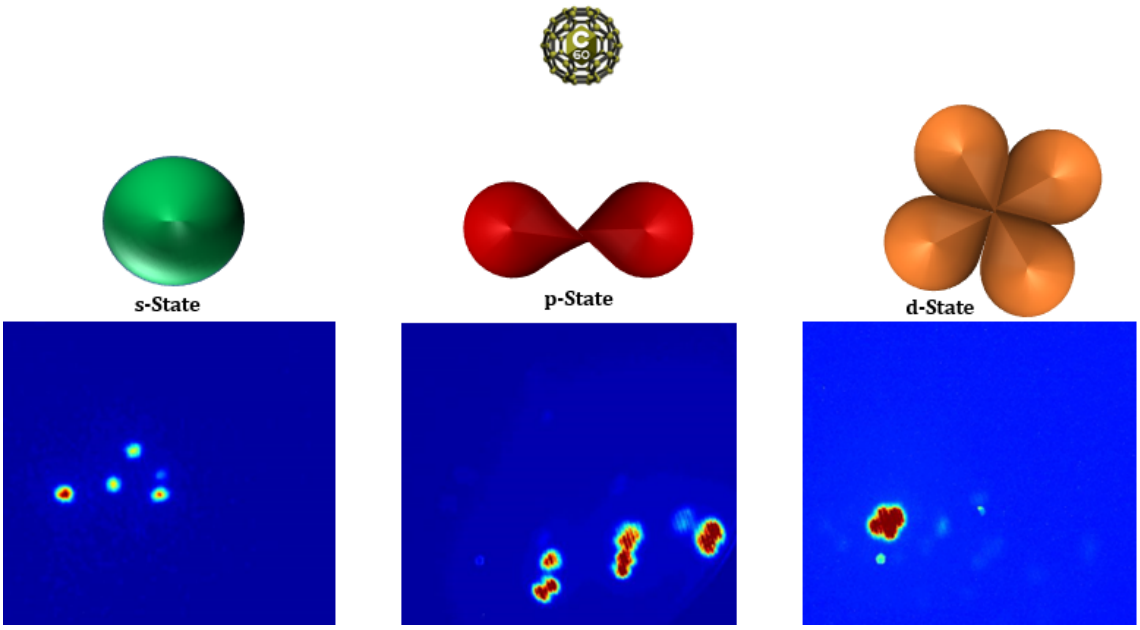

Figure 5.5: C_{60} molecule with possible energy levels shown as our model in the second panel of the figure, while third panel are FEM pictures presenting the corresponding patters appear on the phosphor screen.

5.3 Discovery of the Two-cloverLeaf pattern at Low Coverage Regimes

Up to this point all my previous discussions included the observation of different types of such structures , e.g. (2 and 4-cloverleaves) at high deposition temperatures, i.e. when the lower part of the tip is highly covered with C_{60} molecules. Work in the low coverage regimes was repeated 50 times until finally we observed the formation of such interesting patterns even in the low coverage regimes. In fact **we could detect the 2-Fold Symmetry on the tungsten carbide while it is low covered with** C_{60}; where the low-covered tip here means that features of the tungsten carbide are distinguishable. The FEM picture of this discovery is shown in Fig. 5.6 where the 2-cloverleaf pattern appears on the lower part of the tungsten carbide.

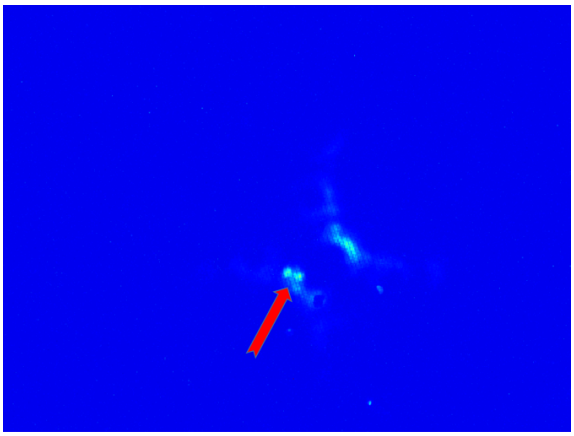

Figure 5.6: FEM picture for the discovery of the formation of a 2-cloverleaf pattern in the low coverage regimes. Features of the tungsten carbide are still visible.

Even though, the previous 2-fold symmetry pattern was obserever at room temperature, it was stable and we could not detect dynamic movements. However, we could do it again and recorded a video for the 2-fold symmetry pattern dynamics, where it is assumed to be rotated. Fig. 5.7 shows FEM picture taken from a video recorded while monitoring this 2-fold symmetry. For each FEM where we could observe a rotation, and we did a model to clarify our observations. The arrows in this model indicate the orientation of the 2-fold symmetry structure. Mainly we could observe three rotational movements represented with the three angles $\theta_1 \approx 48^o$, $\theta_2 \approx 38^o$, and $\theta_3 \approx 103^o$. The time at which each FEM picture was taken and a rotation happened is also recorded at the corresponding model. One Important thing we need to know, is that such dynamics could be observed only at the same position in these low deposition conditions.

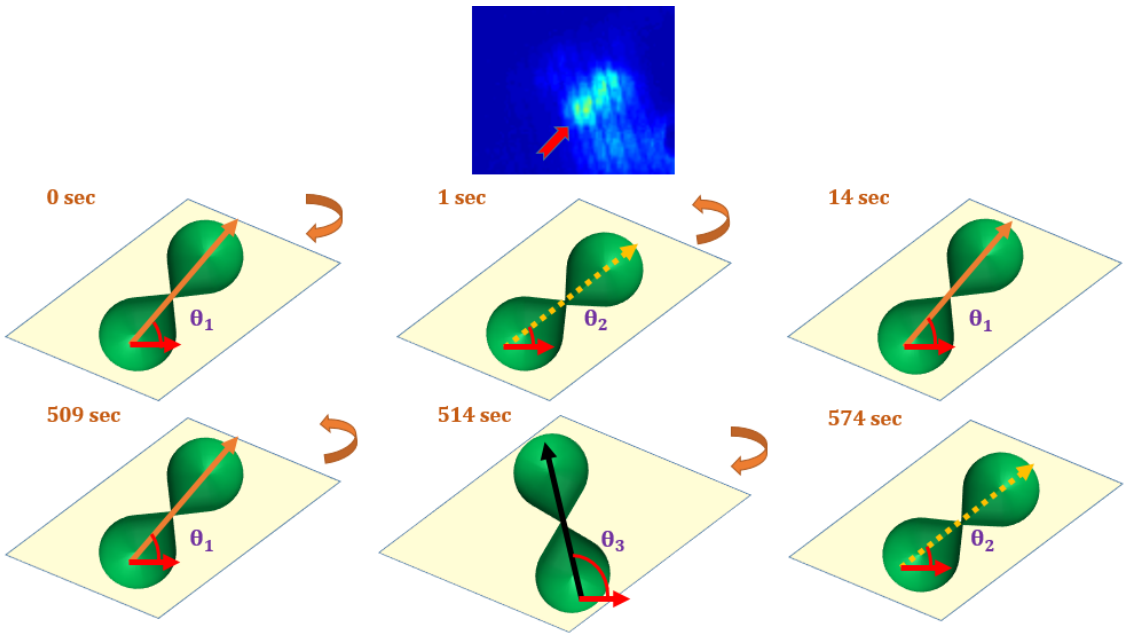

Figure 5.7: FEM picture for the 2-fold symmetry structure (two cloverleaf) on the lower part of the tungsten carbide surface,upper panel with our model represented in the lower two panels. The colored arrows indicate the orientation of the 2-fold symmetry pattern as the three angles show. The time at which each orientation was recorded is also recorded.

Until now we mentioned that we could observe these structures easily in the high coverage regimes without setting constraints. This is true, however we could found a relation between the number of these features and the tip voltage as I am going to illustrate in the next section.

5.4 The Direct Correlation Between the Tip Voltage and the Number of Clover Leaves

At high coverage regimes, every time the experiment was performed similar patterns could be observed regardless of the experimental conditions. Nevertheless, we found a direct relation between the number of these structures, and the applied tip voltage. As we increase the tip voltage and decrease the micro channel plate voltage respectively, the number of these patterns increases as it is shown if Fig. 5.8. Arrows of the same color indicate the appearance or disappearance of one of these structures. As we go through these FEM pictures starting from picture (a) until the final picture (f), the tip voltage has been decreased and so does the number of these features.

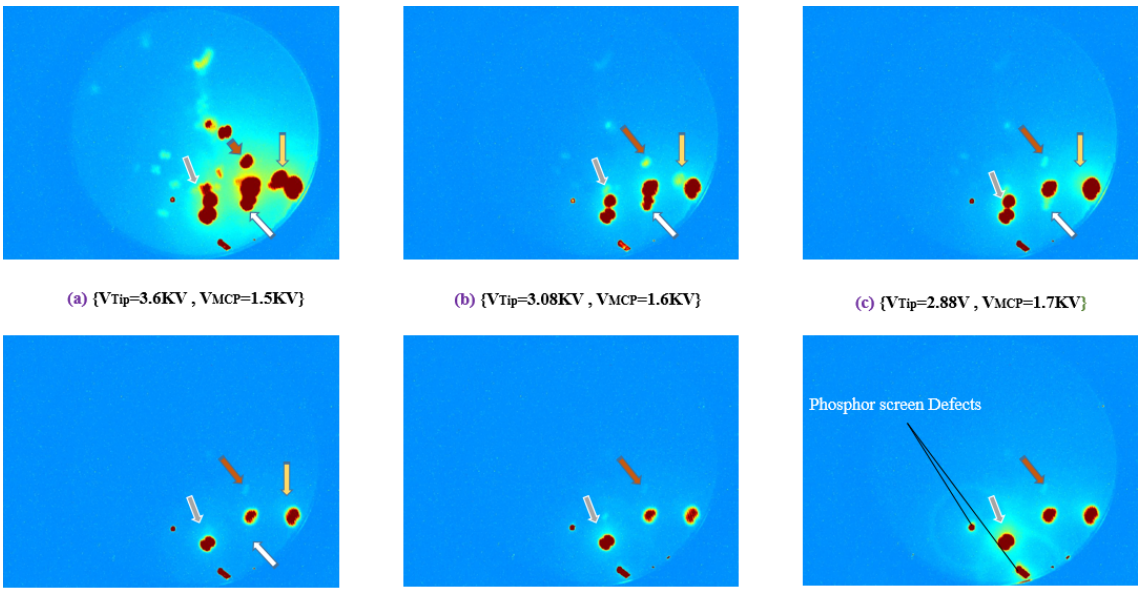

(a) {VTip=3.6KV , VMCP=1.5KV} (b) {VTip=3.08KV , VMCP=1.6KV} (c) {VTip=2.88V , VMCP=1.7KV}

(d) {VTip=2.62KV , VMCP=1.8KV} (e) {VTip=2.5KV , VMCP=1.9KV} (f) {VTip=2.5KV , VMCP=2.0KV}

Figure 5.8: FEM pictures for a highly covered tip, confirming the direct relation between the tip voltage and the number of the spotted structures. Blue means low intensity, while red means high intensity. Pictures are normalised to there highest value to show the number of spots clearly.

In order to understand this correlation we need to check Fig. 2.1. The higher the tip voltage is, the more the deformed potential barrier and the emitted electrons respectively. This means regions where the potential barrier was high such that the voltage is not high enough to overcome this potential barrier we could not see emission from these regions (structures as they are the most likely to emit due to field enhancement). However, by deforming the potential barrier more and more as the applied voltage increases, electrons can now penetrate the barrier from regions (mostly the structures) where it was not possible to penetrate before.

5.5 Dynamics in the High Coverage Regimes

In chapter 3 I showed how stable the field emission Pattern is, in the low and high coverage regimes of a cooled nano-tip. Now at room temperature, by focusing on the high coverage regimes on the tungsten carbide we could see the very dynamical cloverleaf patterns (4-leaf patterns). Fig. 5.9 shows an example of the dynamics of a four-cloverleaf pattern with our model to facilitate imagining the dynamics over time. These FEM pictures were taken from a recorded video and time is also indicated. Even though, the general pattern is still the same, we could observe a rotational movement. Mainly, we could observe two rotational movements going back and forth with respect to the substrate and indicated with the two angles $\Phi_1 \approx 60^o$, and $\Phi_2 \approx 24^o$ in the figure.

To investigate more this 4-cloverleaf pattern at room temperature, we plotted the intensity over time for this structure as it is shown in Fig. 5.10. In this figure we are distinguishing these two patterns, where the left FEM picture of the lower panel represents one case and labeled with our model and a blue star, while the right FEM picture represents the other case labeled with our model and a filled red circle. The blue star in the intensity over time plot indicates the appearance of the pattern labeled with that star, while switching into the other pattern is represented by the filled red circle.

Based on our explanation before, this 4-cloverleaf pattern corresponds to a single C_{60} molecule wave function in the d-state. From a talk of Dr. Yanagisawa, I could understand that a single molecule might vibrate vertically with respect to neighboring molecules. If we use this idea we can explain the fluctuation in the intensity represented in the plot. Where the change in the intensity of FE pattern might be due to the position of this C_{60} molecule with respect to other C_{60} molecules in the same layer. At room temperature the molecule producing this pattern is not stable and might vibrate up and down with respect to the level of C_{60} molecules layer it comes from, resulting in this intensity fluctuations. This is clarified in the model shown in the right part of the lower panel of the figure. In this model the red colored sphere is assumed to be the C_{60} molecule producing that structure as long as it is **not** in the same level of other C_{60} molecules,green spheres, forming that layer of C_{60} molecules. This also might explain the reason of disappearance, and reappearance, of such structure from while to while. If that molecule is above the neighboring molecules we see the clover leaf, however if it goes in between them the structure disappears. Now, the higher this molecule is with respect to its neighboring molecules the stronger the intensity. I will discuss this point in detail later in the next chapter when we cooled down the tip using liquid nitrogen, where we could observe how stable the intensity of FE pattern becomes while cooling the tip (compared to this unstable case at room temperature).

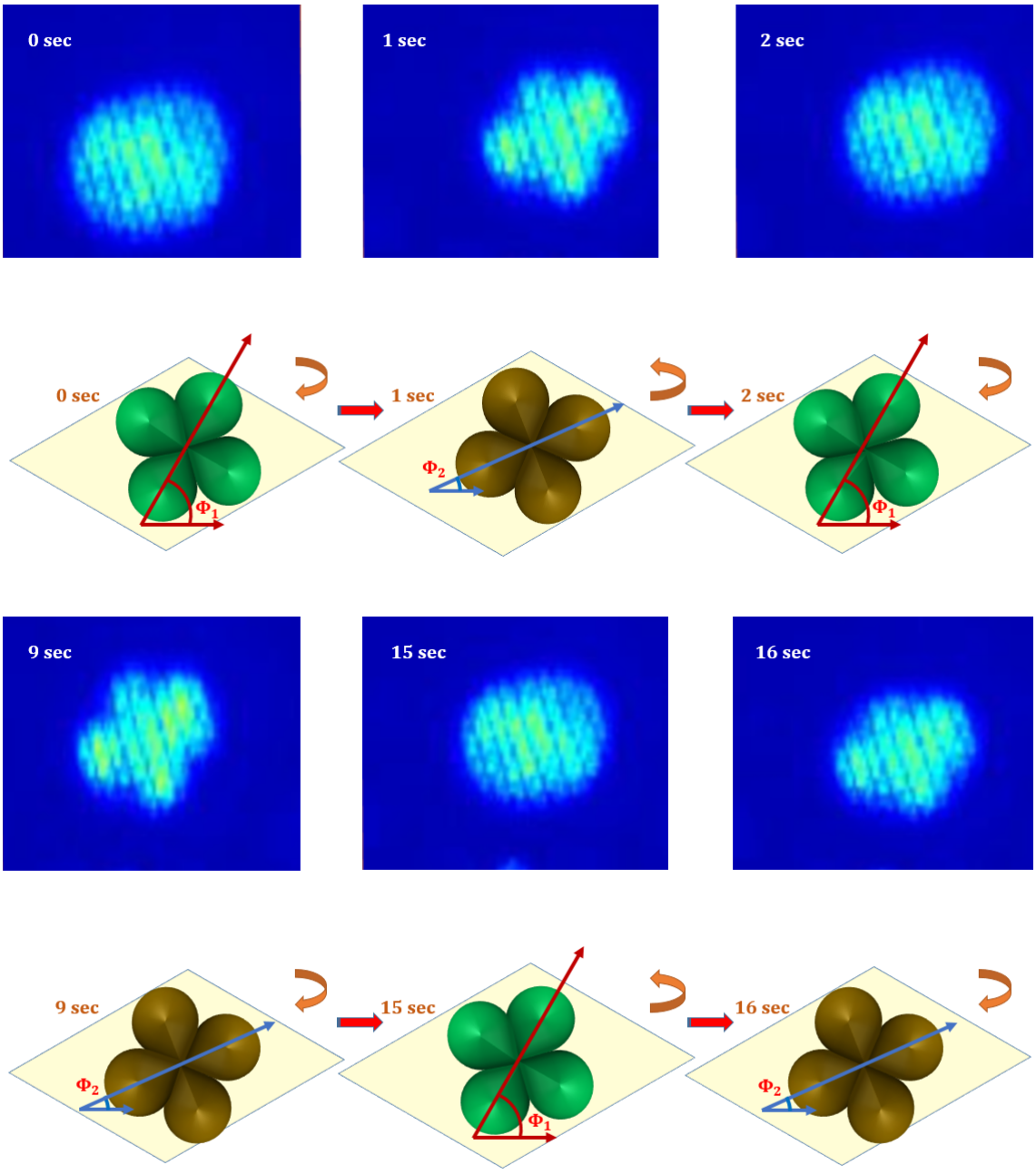

Figure 5.9: FEM pictures for a 4 cloverleaf pattern on a highly covered tungsten carbide surface showing how dynamic are these features were at room temperature (upper panel), and this dynamical structure is modeled in the lower panel to clarify the idea. The time at which each picture was taken is also recorded.

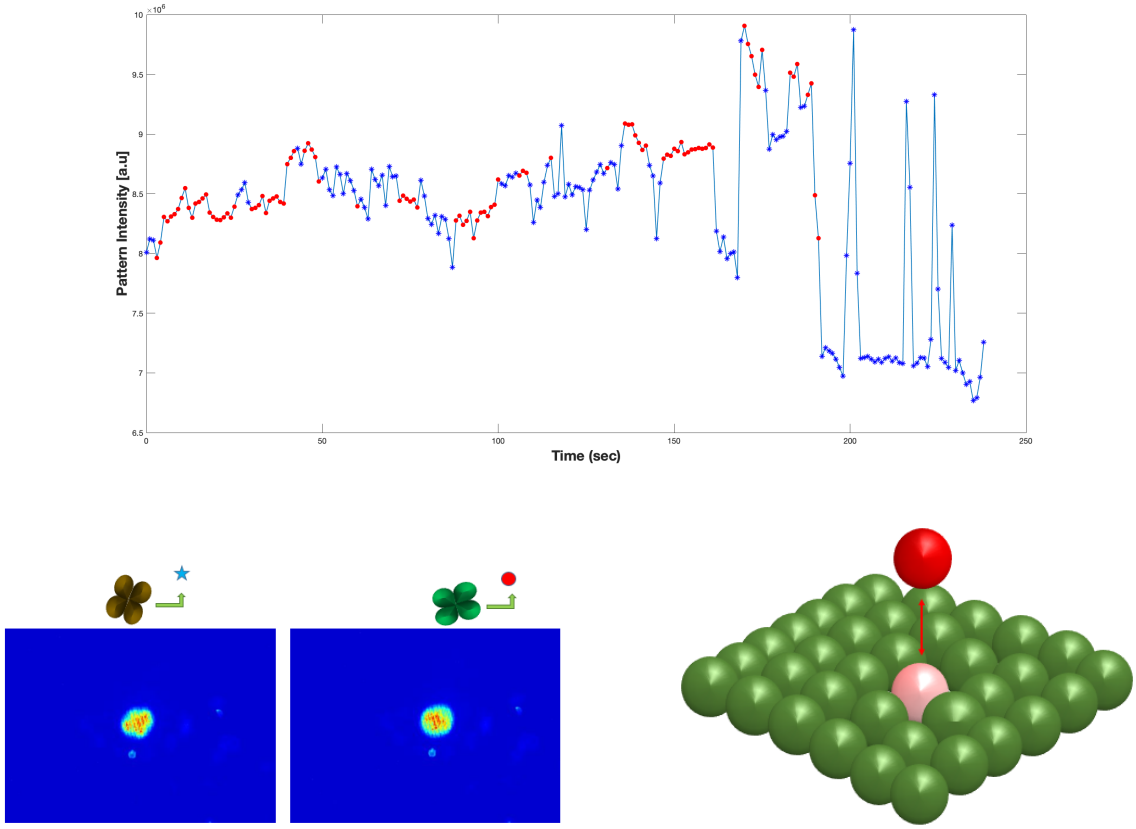

Figure 5.10: The upper panel of the figure shows how the intensity of a FE pattern changes over time for a 4-cloverleaf pattern at room temperature. Two orientations could be observed for the same 4-cloverleaf structure; shown in the left part of the lower panel; each represented with our model and labeled with; a blue star (the left FEM picture); a red filled circle (the right FEM picture). The corresponding label in the intensity-time plot indicates the time at which that pattern has appeared. The right side of the lower panel is a model representing a single C_{60} molecule in the d-state vibrating over a layer of C_{60} molecules causing a fluctuation in the intensity.

Chapter 6

Tip Cooling Via Liquid Nitrogen

Cooling the tip was the main idea of our experiments to reduce the mobilty of C_{60} molecules on the nano-tip hoping to end up with a stable FE pattern. Liquid nitrogen was chosen to do the job, as it is cheap and easy to handle. Mainly, section 4.3 was done completely while the tip has been already cooled down. The method used to cool the tip was discussed in detail in section 3.3.1. Just as a reminder, after filling the cooling tank with liquid nitrogen, the heat is transferred through the cooling elements (ALN and AL_2O_3) into the tip to be cooled down to $\sim$ 90 Kelvin.

6.1 Stability of Field Emission Patterns From Cloverleaves While Cooling a High C_{60}-Covered Tip

As discussed in section 5.2.2 each cloverleaf pattern is considered to represent a single C_{60} molecule due to its wave function nature with specific symmetry based on the symmetry of energy level of that molecule. However, the behaviour of each single C_{60} molecule is not yet known, neither with respect to other molecules nor with respect to the substrate itself. Regardless, whether the cloverleaf pattern originating from a single C_{60} molecule standing over the substrate itself or from a single C_{60} molecule based on its position with respect to other C_{60} molecules. one would expect a decrease in the dynamics of this molecule while cooling the nano-tip. This can not be detected directly. This could be inferred from the intensity of field emission pattern coming from that molecule. At room temperature as the molecule is not stable, we could see a non stability in field emission pattern from that molecule. This is actually demonstrated by the intensity plot shown in Fig. 5.10 for a 4-cloverleaf pattern. The pattern is also illustrated in FEM pictures in Fig. 5.9. While cooling, if the molecule is on the substrate itself, the adhesion of this molecule increases and becomes more stable as the nano-tip temperature decreases. Now, if the molecule is at higher vertical level with respect to its neighbors, it might drop between two of other C_{60} molecules, but still be at a higher vertical level, and becomes more stable. In both cases we expect the intensity of field emission to become steadier as the mobility of the corresponding molecule over the nano-tip decreases while cooling.

To clarify this idea we did the following experiment: we highly covered the nano-tip with C_{60} molecules, at 360 ^{o}C evaporation temperature for 5 minutes with a 500

negatively biased tip at room temperature, and cloverleaf patterns appeared. We focused on one 4-cloverleaf pattern and started cooling the tip using liquid nitrogen. We could observe that the pattern became very stable while cooling. This process took $\sim$ 2.5 hours to reach the minimum possible tip temperature of $\sim$ -180 ^{o}C. We plotted the intensity of field emission current from that 4-cloverleaf pattern as it is shown in Fig. 6.1.

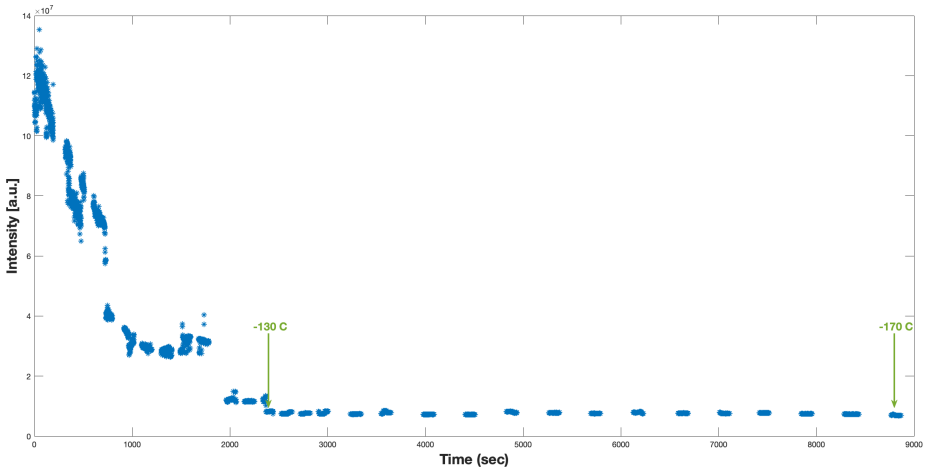

Figure 6.1: Total intensity of a 4-cloverleaf pattern while cooling the tip. Each blue section represents a discrete video recorded. The two green arrows sandwich a region in (Time and Temperature) of constant intensity.

In this experiment we recorded discrete videos for the field emission, where each blue section in the plot represents one of these videos. The two green arrows indicate a region in between where the intensity of the 4-cloverleaf pattern is nearly constant. However, from the beginning of the intensity plot (at room temperate) until $\sim$40 minutes of cooling we can see a drop in the intensity of field emission.

Based on our previous possible explanation in sec. 5.5 and the model presented in Fig. 5.10, this drop in the intensity of field emission could be due to a C_{60} molecule standing at a higher vertical level of other C_{60} molecules of the same layer. Initially the molecule at room temperate will still be moving up and down, and not yet stuck to other C_{60} molecules. When cooled, it becomes more strongly attached to the lower C_{60} molecules, as the sticking coefficient mostly increases while cooling. If we imagine the lower part of C_{60} molecules as a plane, our molecule goes down through this plane while cooling causes a decrease in the field emission pattern intensity. After a while, it will stand constantly in its position to come up with the very stable field emission pattern. Fig. 6.2 is a model explaining this behaviour.

From this model we see how the position of C_{60} molecule (in the d-state) becomes closer to the lower C_{60}-layer covering the tip while cooling, where the sticking coefficient increases. This causes the drop in intensity as one can see in Fig. 6.1, after a while this molecule stands constantly at its position coming up with a constant intensity.

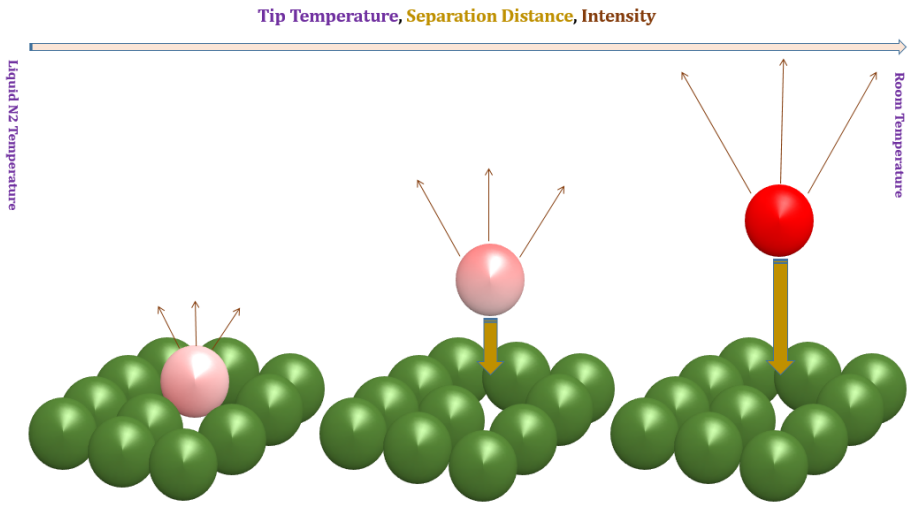

Figure 6.2: A model showing a possible explanation of Fig. 6.1. The red sphere represents a C_{60} molecule responsible for the detected 4-cloverleaf pattern, while green spheres are the lower C_{60} molecules covering the nano-tip.

6.2 F-N Plot Analysis

One of the techniques used to study the behaviour of deposited C_{60} molecules over the nano-tip is F-N plot analysis. It was derived in section 2.6 and shown that the slope of the final plot depends on the work function of the metal and the field enhancement factor. In this section I will discuss the various results we got from different F-N plots taken at room temperature, and after cooling the tip using liquid N_2.

The method used while taking F-N plots is as follows: First, the tip was cleaned by flash heating, then immediately three F-N plots were taken for the clean surface, with time separation of about one minute. After that, different amounts of C_{60} molecules were deposited ending up with a low or highly covered nano-tip. Afterwards, three F-N plots were taken again but now for the covered tip with a relaxation time of roughly one minute between two successive plots. In the following discussion we will see how the behaviour of the covered nano-tip is at different coverage regimes and different temperatures.

6.2.1 Room Temperature-Tip

The surface of the nano-tip was studied at room temperature using the F-N technique. First, I will start this subsection by discussing the low deposition case and then move into the highly covered tip phase.

The upper panel of Fig. 6.3 are FEM pictures of the tip; the left FEM is for the clean surface and the right one is after depositing small amount of C_{60} molecules for **15** minutes. As one can see a circular spot appeared after C_{60} deposition and it is circled with a white circle. Three F-N plots were taken at the corresponding area of the clean surface and averaged as is it shown in the left F-N plot of the lower panel, where $\log(\frac{Intensity of Field Emission}{Voltage^2})$ is plotted over $(\frac{1}{Voltage})$, and a fitting line is plotted over the linear range such that we avoid CCD camera saturation and exclude region where there is no signal to be detected. An average of another three F-N plots where taken at that spotted structural feature after deposition and plotted as it is shown

in the right F-N plot of the lower panel.

This behaviour fulfils our expectations, where as we believe this spotted feature at this low deposition corresponds to a single C_{60} molecule. The existence of such nano-pump molecule could either decrease the work function of the metal or increase the field enhancement factor [19, 21] or do the both at the same time, and based on equation 2.21 we expect to see a decrease in the slope of the fitting line for the F-N plot, and this is what we got and shown by the two fitting lines of the F-N plots in the lower panel of the figure where the slope of the fitting line in the right F-N plot (after deposition) is -41941.0 a.u. which is smaller an absolute value compared to that of the fitting line in the left F-N plot (clean surface) which has a slope of -46893.7 a.u., this is also shown in region number two in the bar diagram of Fig. 6.4.

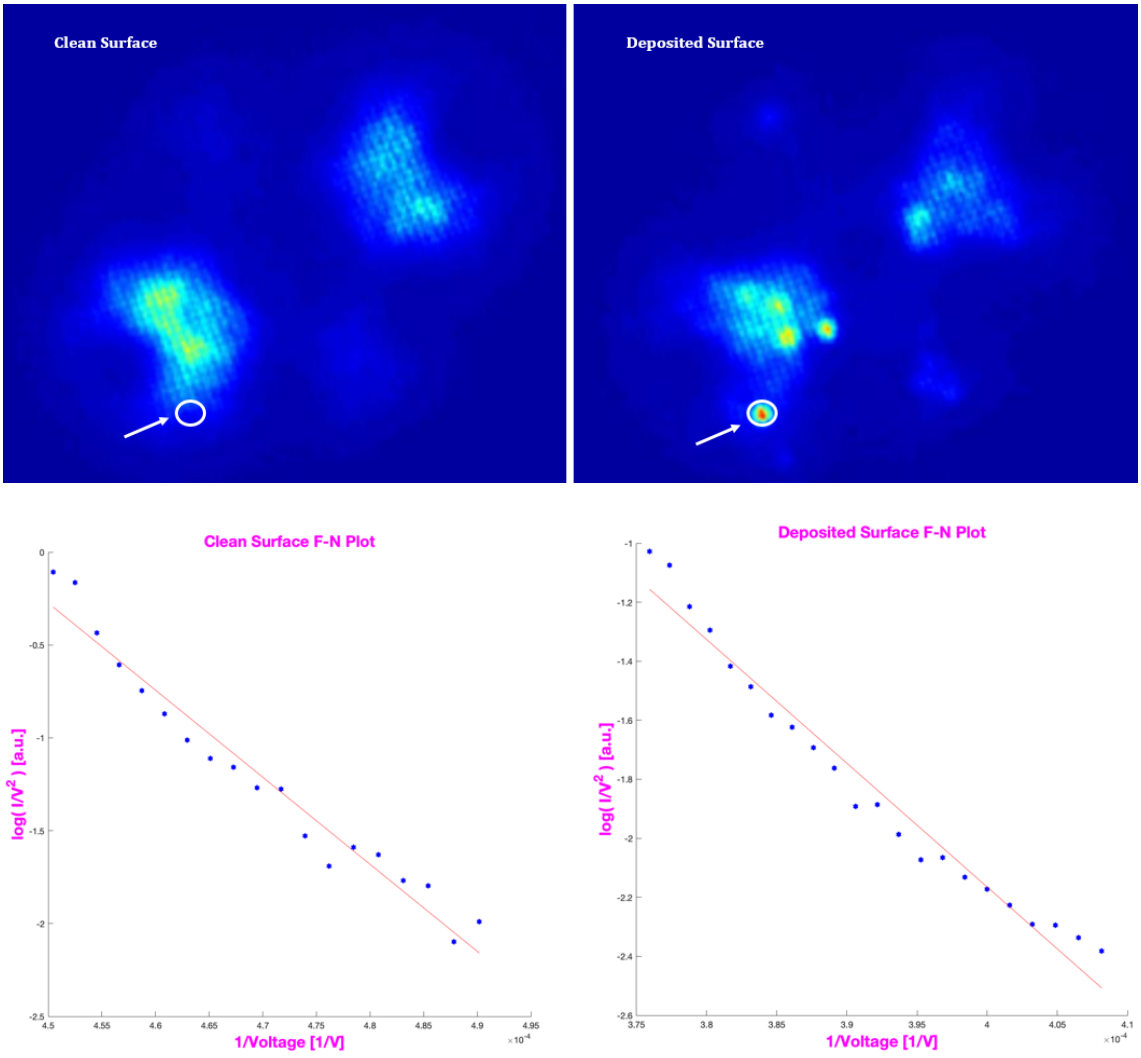

Figure 6.3: The upper panel are FEM pictures; the left is for a clean surface; the right is for a low-C_{60} covered tip; the circled area indicating the appearance of a spotted structure after deposition and to be analyzed using F-N plot technique. The lower panel are F-N plots for that circled region with a fitting line; the left is for the clean surface; the right is after deposition with **a decrease in the slope of the fitting line**.

More tip apex regions were studied using this method at this low deposition case, such that F-N plots were taken before and after C_{60} deposition and the slopes of

the fitting lines were calculated. Fig. 6.4a shows two FEM pictures where the left one is for the clean surface and the right one is for a low-C_{60} covered nano-tip. The regions analyzed are circled with the white circles and numbered. The slopes of the fitting lines of the F-N plots for these circled areas are shown in the bar diagram in Fig. 6.4b, where each green bar corresponds to the slope of an average of three F-N plots taken from a clean surface, while a red bar corresponds to the slope of an average of another three F-N plots for the same region after C_{60} deposition. Each one of these two successive bars labeled with a number corresponds to a region in the FEM pictures with the same number in Fig. 6.4a.

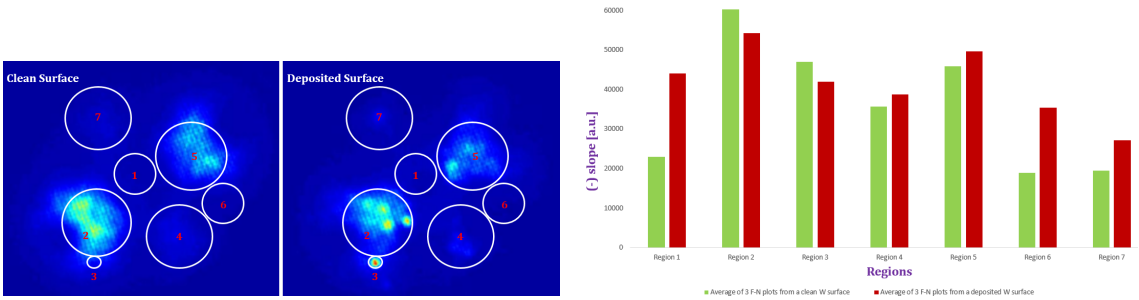

(a) (b)

Figure 6.4: FEM pictures for the clean and **a low-C_{60} covered** nano-tip **at room temperature** (a) with circled and numbered areas to be analyzed using F-N method. (b) is a bar diagram for the slopes of the fitting lines for the clean and covered regions labeled with the corresponding areas.

From this bar diagram we can see a decrease in the slope in regions (2 and 3) where the spotted structures appeared, and this coincides our expectations for the decrease in the work function and an increase in the field enhancement factor wherever a nano-pump exists. In the remaining regions where no such structures appearing, we can see an increase in the slope which might be due to a decrease in the field enhancement factor due to contamination and degradation specially after depositing for 15 minutes.

The previous analysis was just for a small amount of C_{60} covering the nano-tip. We did a similar kind of experiments but for a highly covered nano-tip with C_{60} molecules. Fig. 6.5 shows our results, where the left FEM pictures are for the clean and highly deposited nano-tip, and the analyzed regions are also labeled with white circles and red numbers. The tip was flashed and the slope of an averaged three F-N plots was calculated and shown in the green bars. Then, C_{60} was evaporated at high evaporation temperature for 15 minutes, and again three F-N plots were taken and the slope of their average is shown in the red bars of the figure.

The behaviour is different compared to the low-covered tip case. Mainly we could observe an increase in the slope of the F-N plots as the bar diagram shows, even when we have a spotted structure as in regions (8,3,9 and 2) which is opposite to what we found in the low coverage case discussed before. It seems to be that these spots in the high coverage case might be not due to a single C_{60} molecule. Interestingly, we can see a decrease in the slope in regions (1 and 7). At these two regions there might be a single C_{60} molecule such that emission from it caused this decrease in slope, and we are not able to notice this emission since these two facets have higher local work functions compared to neighboring facets, and the applied

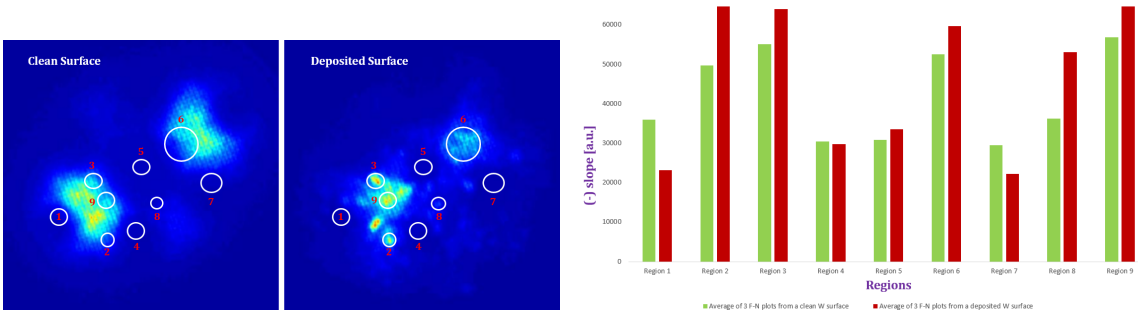

(a) (b)

Figure 6.5: FEM pictures for the clean and **a high-C_{60} covered** nano-tip **at room temperature** (a) with circled and numbered areas to be analyzed using F-N method. (b) is a bar diagram for the slopes of the fitting lines for the clean and covered regions labeled with the corresponding areas.

voltage is not enough to trigger high emission from them or from C_{60} molecules covering them as from other more intense facets.

6.2.2 Cooled Tip Via Liquid N_2

Now it is time to study the behaviour of a nano-tip covered with C_{60} at low temperatures. We cooled the tip by filling the liquid N_2 tank and deposited different amounts of C_{60}. First I will discuss the low deposition case and then show the results from a highly covered tip.

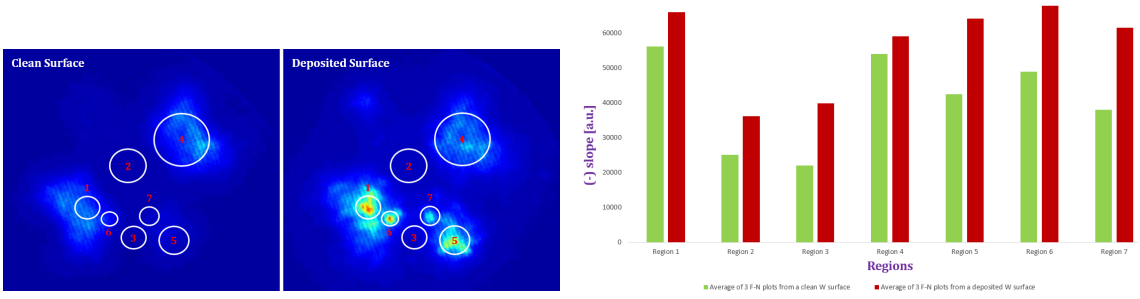

(a) (b)

Figure 6.6: FEM pictures for the clean and **a low-C_{60} covered cooled nano-tip** (a) with circled and numbered areas to be analyzed using F-N method. (b) Is a bar diagram for the slopes of the fitting lines for the clean and covered regions labeled with the corresponding areas.

If we compare this bar diagram with that of the low deposition at room temperature, we can see a different behaviour. Even at the spotted structures which we propose at this low evaporation temperatures to be single C_{60} molecules, an increase in the slopes happened. A possible explanation for this is that a large decrease might have happened for the enhancement factor due to cooling, and overcame the decrease in the work function such that an overall increase happened for the slopes.

By increasing the amount of C_{60} deposited we could observe mainly a decrease in the slopes from most of the regions analyzed as it is shown in the bar diagram of Fig. 6.7, except region 6. Depositing over a cooled nano-tip might put C_{60} molecules closely to each other with very small spaces, and increases the probability of having single C_{60} molecules to work as bumps over the lower C_{60} layer, and in this case we might have a larger decrease in the work function compared to the decrease in the enhancement factor do to cooling, coming up with a drop in the slopes of the fitting

lines. However, the jump in the work function in region 6 might come from a sharp drop in the enhancement factor.

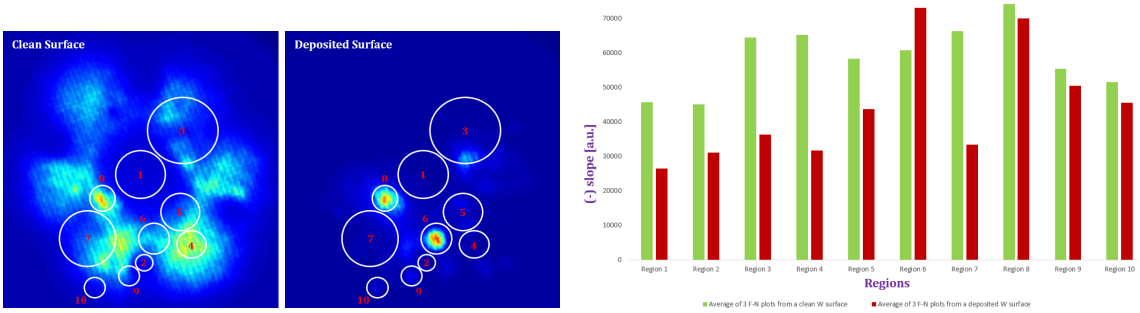

(a) (b)

Figure 6.7: FEM pictures for the clean and **a highly-C_{60} covered cooled nano-tip** (a) with circled and numbered areas to be analyzed using F-N method. (b) Is a bar diagram for the slopes of the fitting lines for the clean and covered regions labeled with the corresponding areas.

6.3 Random Behaviour of F-N Plot's Slope

In the previous section we tried to characterize tip surface based on the results we got from F-N plot slopes. We studied the low and high C_{60} covered nano-tip at both room and low temperatures. In fact, we analyzed more data at these conditions and determined the slopes of F-N plots. Previous studies at room temperature [53] showed a widely scattered data for the slopes of F-N plots. In this section we compare the behaviour of slopes taken at room and at low temperatures.

The bar diagram in Fig. 6.8 compares the slopes of F-N plots taken from different regions at room temperature. Each green bar represents the slope of an average of three F-N plots taken from the clean surface, while the red bar corresponds to the slope of an average of three plots after deposition. The lower panel shows FEM pictures for four deposition cases to represent our results. Selected regions where spots appeared were chosen and the slope of F-N plots was determined from circular area including that spot. As one can see, an increase in the slopes of F-N plots happened from spots labeled with numbers (1,2 and 4), while a decrease in the slope was recorded from spot 3 where these represent low deposition case. However, from the analysed spots in the high deposition case, it seems like there is a tendency of an increase in the slopes as it is shown from regions (5,6,7,8 and 9).

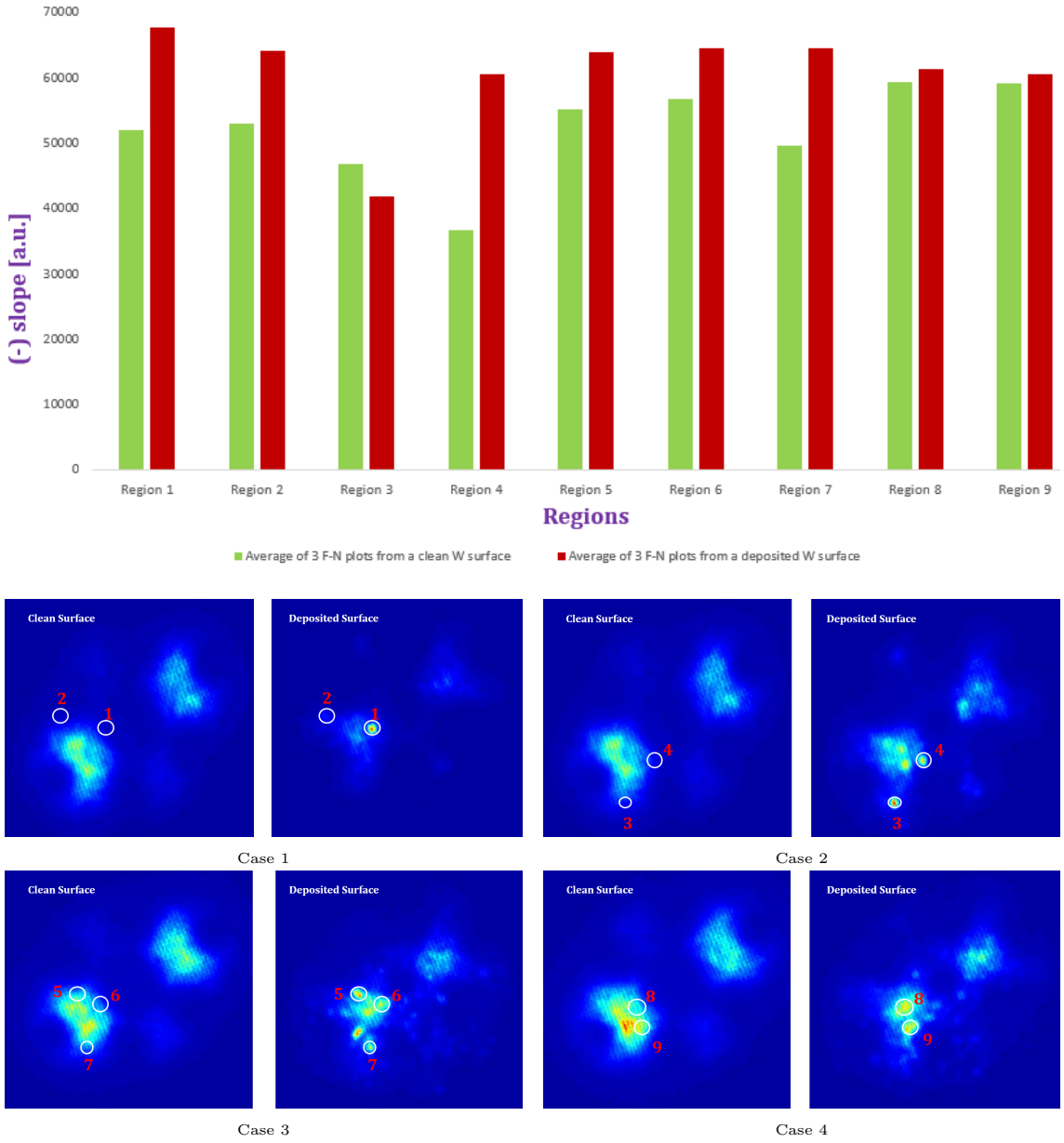

Figure 6.8: Random behaviour of the slopes retrieved by several F-N plots (bar diagram) **at room temperature**. FEM pictures in the lower panel show investigated areas labeled with the corresponding areas in the bar diagram, for four chosen deposition cases. Dark blue areas show low emission areas while light blue areas show higher intensity.

Similar kind of experiments were also done on a cooled nano-tip. Now, C_{60} molecules are very stable on the tip, and hence more spots could be detected and analyzed using F-N plots. Fig. 6.9 shows the random behavior of the slopes of F-N plots in the bar diagram taken for spots observed on the phosphor screen. Four deposition cases where analyzed and investigated regions are labeled in the FEM pictures shown in the lower panel of the figure. From the bar diagram, we see an increase in the slope of F-N plots from regions (1,2 and 4) in the low deposition case, while a drop in the slope is observed from region 3. We also see an increase in the slope in the high deposition cases in regions (6,8 and 9) while again a decrease in the slope happened from regions (5 and 7).

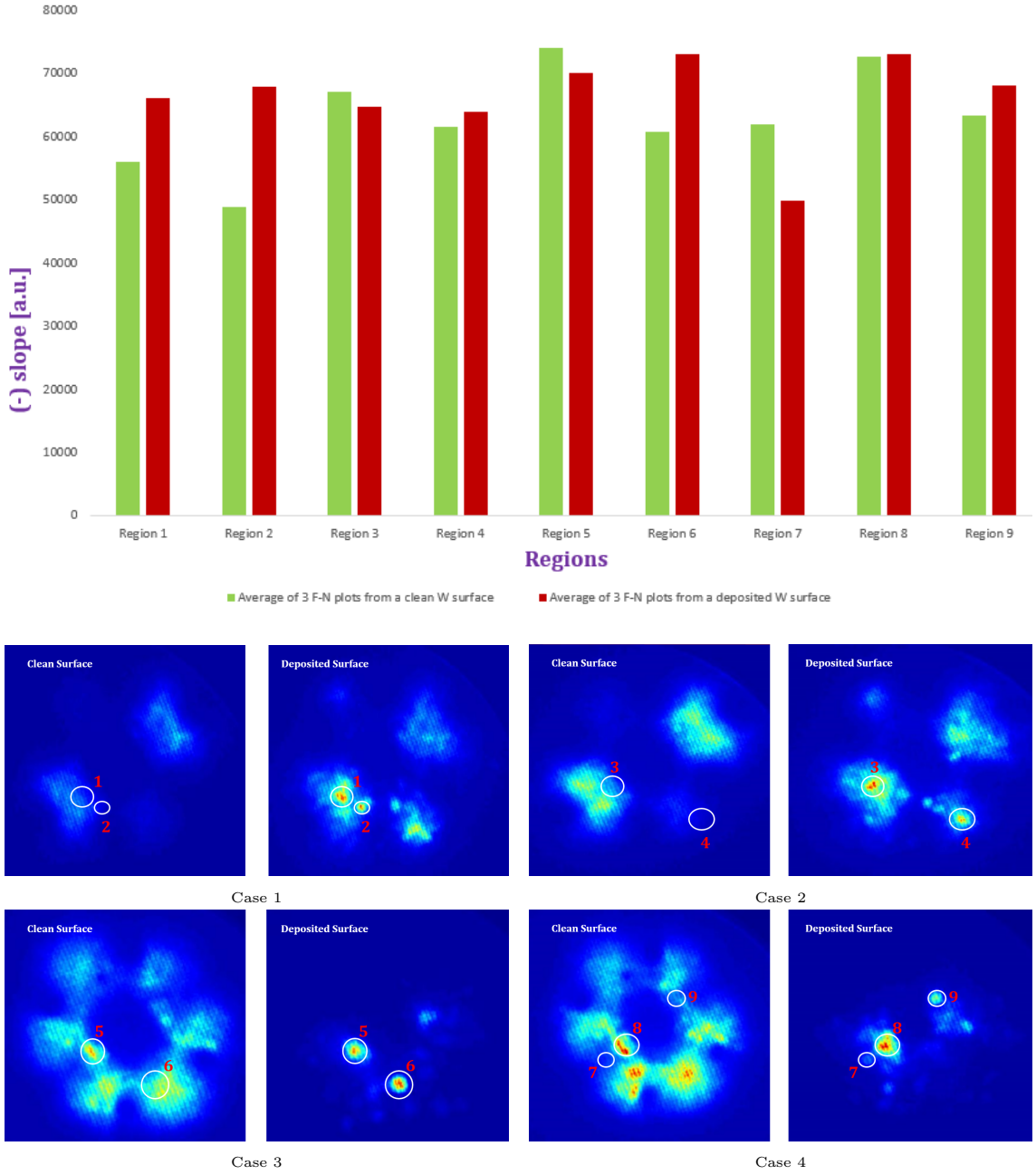

Figure 6.9: Random behaviour of the slopes retrieved by several F-N plots (bar diagram) **at low temperature**. FEM pictures in the lower panel show investigated areas labeled with the corresponding areas in the bar diagram, for four chosen deposition cases. Dark blue areas show low emission areas while light blue areas show higher intensity.

This random behavior in the slopes of the F-N plots at room temperature and at low temperatures proposes that F-N plot is not affected by the mechanical stability of C_{60} molecules.

Chapter 7

Summary and Outlook

The main goal of this thesis was to stabilize field emission patterns to provide better conditions that can help to find out the mechanism forming the cloverleaves, where each cloverleaf is considered to represent a single C_{60} molecule.

Different amounts of C_{60} were deposited onto the nano-tip. We examined how the pattern gradually transferred from a cleaned tungsten surface, into a clean tungsten carbide surface. We investigated the behaviour of C_{60} molecules over these two kind of surfaces. At high coverage regimes we observed the formation of cloverleaf patterns in a reproducible manner. We also discovered the formation of a 2-cloverleaf pattern for the first time on the tungsten carbide surface in the low coverage regime. We cooled the tip via a newly designed cooling system using liquid nitrogen and observed that FE patterns corresponding to C_{60} molecules became very stable at low temperature. We also analysed different structures we could detect on the phosphor screen by determining slopes of F-N plots for electron emission from single C_{60} molecules on the nano-tip and compared them with the slopes of F-N plots taken from the corresponding clean surface. At room temperature, our study matched the previous study where we could observe a random behavior in the slopes of F-N plots. At low temperatures, we also observed the random behavior of the F-N slopes indicating that F-N plot is not affected by the mechanical stability of C_{60} molecules.

From this research and after cooling a C_{60} covered nano-tip we could stabilize the cloverleaf patterns by reducing the mobility of C_{60} molecules on the nano-tip. As the origin of these patters is not yet known, the result of our research might help to find out the origin of these cloverleaves. We propose that each one of these cloverleaves is correlated to the wave function nature of a single molecule. This opens a door for a future experiment where laser light could be used to illuminate the stable C_{60} molecules deposited on the cooled nano-tip. If one succeeds to transfer from a circular spot into a two clover leaf, and a four clover leaf pattern respectively, this will support our proposal, since a laser in this case acts as an energy exciter for molecules and could excite a single C_{60} molecule into a higher energy level with its own wave function symmetry. A circular spot in this scenario corresponds to a single C_{60} molecule in the s-state and the two-leaf pattern corresponds in turn to the same but excited C_{60} molecule. The most interesting structure,namely the four-leaf pattern, comes after exciting a single C_{60} molecule already in the p-state.

Bibliography

[1] R. W. Wood. "A New Form of Cathode Discharge and the Production of X-Rays, together with Some Notes on Diffraction. Preliminary Communication". In: *Phys. Rev. (Series I)* 5 (1 July 1897), pp. 1–10.

[2] JE Lilienfeld. "The Radiation Radiation of the Cathode during the Auto-electronic Discharge (Lecture at the German Physics Day in Leipzig, 17.-24.9.1922)". In: *Physical Journal* 23.22/23 (1922), pp. 506–511.

[3] W Schottky. "about cold and warm electron discharges". In: *Journal of Physics A Hadrons and Nuclei* 14.1 (1923), pp. 63–106.

[4] B. S. Gossling. "The emission of electrons under the influence of intense electric fields". In: *Phil. Mag.* 1.3 (1926), pp. 609–635.

[5] R. A. Millikan and Carl F. Eyring. "Laws Governing the Pulling of Electrons out of Metals by Intense Electrical Fields". In: *Phys. Rev.* 27 (1 Jan. 1926), pp. 51–67.

[6] Robert A. Millikan and Charles C. Lauritsen. "Dependence of Electron Emission from Metals Upon Field Strengths and Temperatures". In: *Phys. Rev.* 33 (4 Apr. 1929), pp. 598–604.

[7] Ralph Howard Fowler and Lothar Nordheim. "Electron emission in intense electric fields". In: *Proceedings of the Royal Society of London. Series A, Containing Papers of a Mathematical and Physical Character* 119.781 (1928), pp. 173–181.

[8] LW Nordhiem. "The effect of the image force on the emission and reflexion of electrons by metals". In: *Proceedings of the Royal Society of London. Series A, Containing Papers of a Mathematical and Physical Character* 121.788 (1928), pp. 626–639.

[9] Erwin W Müller. "Elektronenmikroskopische beobachtungen von feldkathoden". In: *Zeitschrift für Physik* 106.9-10 (1937), pp. 106, 541.

[10] Erwin W M. "Further observations with the field electron microscope". In: *Journal of Physics* 108.9-10 (1938), pp. 108, 668.

[11] Leonhard Grill and Christian Joachim. *Imaging and Manipulating Molecular Orbitals: Proceedings of the 3rd AtMol International Workshop, Berlin 24-25 September 2012*. Springer Science & Business Media, 2013.

[12] Allan J Melmed and Erwin W Müller. "Study of molecular patterns in the field emission microscope". In: *The Journal of Chemical Physics* 29.5 (1958), pp. 1037–1041.

[13] RJ Hill and PWM Jacobs. "Note on the Observation of Molecules by Field Emission Microscopy". In: *The Journal of Chemical Physics* 30.3 (1959), pp. 853–854.

[14] Robert Gomer and Donald A Speer. "Molecular images with the projection microscope. The ionization potential of Zinc Phthalocyanine". In: *The Journal of Chemical Physics* 21.1 (1953), pp. 73–80.

[15] JA Becker and RG Brandes. "A Favorable Condition for Seeing Simple Molecules in a Field Emission Microscope". In: *Journal of Applied Physics* 27.3 (1956), pp. 221–223.

[16] Robert Gomer. "Field emission, field ionization, and field desorption". In: *Surface science* 299 (1994), pp. 129–152.

[17] Robert Gomer. "Field Emission Microscopy and Some Applications to Catalysis and Chemisorption". In: *Advances in Catalysis*. Vol. 7. Elsevier, 1955, pp. 93–134.

[18] Hirofumi Yanagisawa et al. "Optical control of field-emission sites by femtosecond laser pulses". In: *Physical review letters* 103.25 (2009), p. 257603.

[19] Hirofumi Yanagisawa et al. "Laser-induced asymmetric faceting and growth of a nano-protrusion on a tungsten tip". In: *Apl Photonics* 1.9 (2016), p. 091305.

[20] R Gomer. *Field Emission and Field Ionization, vol. 9 of Harvard Monographs in Applied Science*. 1961.

[21] DJ Rose. "On the magnification and resolution of the field emission electron microscope". In: *Journal of Applied Physics* 27.3 (1956), pp. 215–220.

[22] Dilip S, Mahendra A, and Farid Jamali Sheini. "Field Emission from Nanowires". In: July 2011. ISBN: 978-953-307-318-7.

[23] Olivier L Guise et al. "Reproducible electrochemical etching of tungsten probe tips". In: *Nano Letters* 2.3 (2002), pp. 191–193.

[24] M Klein and G Schwitzgebel. "An improved lamellae drop-off technique for sharp tip preparation in scanning tunneling microscopy". In: *Review of scientific instruments* 68.8 (1997), pp. 3099–3103.

[25] JP Ibe et al. "On the electrochemical etching of tips for scanning tunneling microscopy". In: *Journal of Vacuum Science & Technology A: Vacuum, Surfaces, and Films* 8.4 (1990), pp. 3570–3575.

[26] DK Biegelsen et al. "Ion milled tips for scanning tunneling microscopy". In: *Applied physics letters* 50.11 (1987), p. 696.

[27] J Garnaes et al. "Transmission electron microscopy of scanning tunneling tips". In: *Journal of Vacuum Science & Technology A: Vacuum, Surfaces, and Films* 8.1 (1990), p. 441.

[28] J Méndez, M Luna, and AM Baro. "Preparation of STM W tips and characterization by FEM, TEM and SEM". In: *Surface science* 266.1-3 (1992), pp. 266, 294.

[29] E Paparazzo et al. "Effects of HF attack on the surface and interface microchemistry of W tips for use in the STM microscope: a scanning Auger microscopy (SAM) study". In: *Vacuum* 52.4 (1999), p. 421.

[30] AI Oliva et al. “Electrochemical preparation of tungsten tips for a scanning tunneling microscope”. In: *Review of scientific instruments* 67.5 (1996), p. 1917.

[31] Luca Ottaviano, Luca Lozzi, and Sandro Santucci. “Scanning Auger microscopy study of W tips for scanning tunneling microscopy”. In: *Review of scientific instruments* 74.7 (2003), p. 3368.

[32] C Julian Chen. *Introduction to scanning tunneling microscopy*. Vol. 4. Oxford University Press on Demand, 1993.

[33] HS Kim et al. “Oxygen processed field emission tips for microcolumn applications”. In: *Journal of Vacuum Science & Technology B: Microelectronics and Nanometer Structures Processing, Measurement, and Phenomena* 11.6 (1993), p. 2327.

[34] Vu Thien Binh et al. “Sharpening of metal tips by heat treatment in vacuum”. In: *Journal of Physics E: Scientific Instruments* 9.5 (1976), p. 377.

[35] A Piquet et al. “A determination of the surface self-scattering coefficient with spikes a field mission (tungst ‘e ne)”. In: *Surface Science* 44.2 (1974), p. 575.

[36] Erwin W Müller. “Resolution of the atomic structure of a metal surface by the field ion microscope”. In: *Journal of Applied Physics* 27.5 (1956), pp. 474–476.

[37] MJ Southon. “Field emission and field ionization”. In: *Field-Ion Microscopy*. Springer, 1968, pp. 6–27.

[38] Charles Kittel. “Introduction to solid state physics, John Wiley & Sons”. In: *Inc., New York* (2005).

[39] BJ Hopkins and KR Pender. “The work function of a (110) oriented tungsten single-crystal face”. In: *British Journal of Applied Physics* 17.2 (1966), p. 281.

[40] Yue Wang et al. “Local work functions of clean tungsten surfaces under electric fields based on ab initio calculations”. In: *2019 International Vacuum Electronics Conference (IVEC)*. IEEE. 2019, pp. 1–2.

[41] ME Lin et al. “Electron emission from an individual, supported C 60 molecule”. In: *Physical Review B* 47.12 (1993), p. 7546.

[42] J Abrefah et al. “Vapor pressure of Buckminsterfullerene”. In: *Applied Physics Letters* 60.11 (1992), pp. 1313–1314.

[43] V Piacente et al. “Vapor pressure of C60 buckminsterfullerene”. In: *The Journal of Physical Chemistry* 99.38 (1995), pp. 14052–14057.

[44] CS Sundar et al. “Thermal decomposition of C60”. In: *Solid state communications* 84.8 (1992), pp. 823–826.

[45] Ying Wang et al. “Thermal decomposition of polymeric C60”. In: *Chemical physics letters* 217.4 (1994), pp. 413–417.

[46] MAK Zilani et al. “Adsorption and thermal decomposition of C60 on Co/Si (111)-7× 7”. In: *Applied surface science* 253.10 (2007), pp. 4554–4559.

[47] MR Stetzer et al. “Thermal stability of solid C 60”. In: *Physical Review B* 55.1 (1997), p. 127.

[48] Thomas Wågberg et al. “A Raman study of polymerised C60”. In: *Applied Physics A* 64.3 (1997), pp. 223–226.

[49] Rainer D Beck et al. “Formation of C119 by Thermal Decomposition of C60O”. In: *The Journal of chemical physics* 102.1 (1995), pp. 540–543.

[50] Takahiro Matsumoto et al. “Field Emission from Graphene Nanosheets”. In: *Graphene Simulation*. IntechOpen, 2011.

[51] Yoichiro Neo et al. “Revealing real images of cloverleaf pattern emission sites by using field ion microscopy”. In: *Journal of Vacuum Science & Technology B, Nanotechnology and Microelectronics: Materials, Processing, Measurement, and Phenomena* 28.2 (2010), C2A1–C2A4.

[52] Wei Chen et al. “Molecular orientation-dependent ionization potential of organic thin films”. In: *Chemistry of Materials* 20.22 (2008), pp. 7017–7021.

[53] Hiroshi Morikawa et al. “Current-voltage characteristics of field electron emission through phthalocyanine molecules on a tungsten field emitter”. In: *Japanese journal of applied physics* 36.5A (1997), p. L583.